Electronic Supplementary Material (ESI) for Physical Chemistry Chemical Physics.

Electronic Supporting Information

Structure, ligands and substrate coordination of the oxygen-evolving complex of photosystem II in the S_2 state: a combined EPR and DFT study

Thomas Lohmiller,[a] Vera Krewald,[a] Montserrat Pérez Navarro,[a] Marius Retegan,[a] Leonid Rapatskiy,[a] Mark Nowaczyk,[b] Alain Boussac,[c] Frank Neese,[a] Wolfgang Lubitz,[a] Dimitrios A. Pantazis*[a] and Nicholas Cox*[a]

[a]*Max-Planck-Institut für Chemische Energiekonversion, Stiftstrasse 34-36, D-45470 Mülheim an der Ruhr, Germany. Fax: +49 208 306 3955; Tel: +49 208 306 3552; E-mail: dimitrios.pantazis@cec.mpg.de; nicholas.cox@cec.mpg.de*

[b]*Ruhr-University Bochum, Universitätsstrasse 150, D-44780 Bochum, Germany.*

[c]*iBiTec-S, URA CNRS 2096, CEA Saclay, 91191 Gif-sur-Yvette, France.*

Table of contents

S1 PSII sample preparation

In native and Sr^{2+} substituted samples, the S_2 state was generated by short white-light illumination (5 s) with a tungsten lamp at 200 K, , using an ethanol bath cooled with dry ice.

Ammonia was added to the samples as follows. A stock solution of 1 M ammonium chloride ($^{14}NH_4Cl$) in 1 M HEPES buffer set to a pH of 7.5 was made. For Q- and W-band samples, this solution was then added to the photosystem II (PSII) sample at a ratio of 1:10 (*v*/*v*), yielding a concentration of the free base NH_3 of 2 mM. The samples were reconcentrated using Millipore microcentrifuge filters to the desired concentration. Afterwards, the sample was placed in a Q- or W-band tube, left in complete darkness for ≈10 min and frozen for experiments in the S_1 state. To generate the NH_3-modified S_2 state, the sample was first illuminated at 200 K for 5 s and then subsequently annealed at ≈260 K (ethanol/dry ice) for 20-30 s before freezing to 77 K (liquid N_2). A similar procedure was used for X-band samples. Here though, the PSII sample was placed in the X-band tube and given two saturating light flashes prior to the addition of $^{14}NH_4Cl$ solution. There was a one-hour delay between the two light flashes and the addition of NH_3, during which the sample was kept in complete darkness. Phenyl-p-benzoquinone (PPBQ) dissolved in dimethyl sulfoxide (DMSO) was added to the sample immediately prior to the addition of $^{14}NH_4Cl$ solution. After incubation for 2-3 min, the sample was frozen to first record spectra in the dark-adapted state. Subsequent illumination at 180 K (ethanol/liquid N_2) followed by an annealing step at 0 °C (ice/water) for 10-20 s generated the NH_3-modified S_2 state.

S2 Data processing: baseline correction and light-minus-dark subtraction

To minimize possible contributions from underlying signals from other paramagnetic species in the sample, such as hexaquo-Mn^{II}, oxidized cytochrome b_{559} and c_{550} and Fe^{II}/Q_A^-, S_2-minus-S_1 (light-minus-dark) subtractions were performed for X- and Q-band pulse EPR and electron nuclear double resonance (ENDOR) spectra. From derivative-shaped, *i.e.* continuous wave (CW) or pseudo-modulated, EPR spectra a fitted baseline was subtracted.

Three-pulse electron spin echo envelope modulation (ESEEM) data were also baseline-corrected after light-minus-dark subtraction of the normalized time-domain traces. (Fig. S1), in order to obtain spectra containing only resonances from the oxygen-evolving complex (OEC) in the S_2 state, excluding modulations from other paramagnetic species, foremost the background cytochrome (^{14}N) signals. The (T_1) decay was modeled and removed by subtracting a third (X-band), a fifth (Q-band Mn_4O_5Ca, Mn_4O_5Sr) or seventh (Q-band Mn_4O_5Ca–NH_3) order polynomial fit function from the light-minus-dark difference.

Hyperfine sublevel correlation (HYSCORE)-spectroscopic data were baseline corrected using polynomial fit curves in both dimensions. Before Fourier transformation, a hamming apodization window and zero-filling were applied to the individual ESEEM and HYSCORE spectra. Experimental and simulated X-band ESEEM spectra were normalized with respect to the time domain spectra. Frequency-domain HYSCORE spectra and simulations were normalized with respect to the height of the single-quantum ^{14}N peaks.

Electron electron double resonance (ELDOR)-detected NMR (EDNMR) spectra were baseline-subtracted and further processed to obtain an ENDOR-like representation of the spectra as described in Ref.[1].

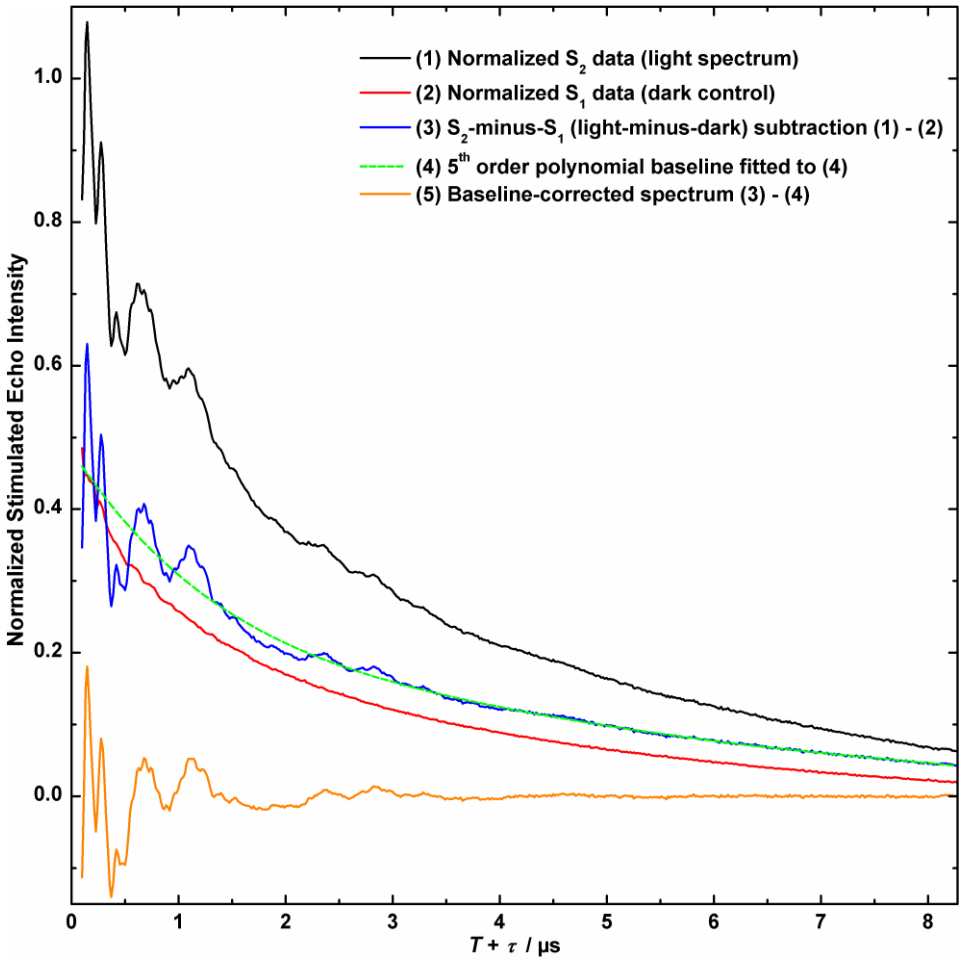

Fig. S1 Example for the light-minus-dark subtraction and baseline correction of three-pulse ESEEM spectra. The solid black and red lines depict ESEEM spectra of a PS II sample in the S_2 (1) and S_1 states (2), after subtraction of the y-axis offset and normalization. The blue solid line shows the spectrum resulting from the S_2-minus-S_1 subtraction (3). The superimposing green dashed line (4) represents a fifth order polynomial fit curves to (3). The solid orange line (5) is the baseline-corrected resulting ESEEM spectrum after background subtraction. Experimental parameters: magnetic field: 1220 mT, τ: 260 ns; other settings were those given in Fig. S4.

S3 Spectral simulations

The EasySpin[2, 3] function 'pepper' was used to calculate EPR spectra, 'salt' for ENDOR, 'saffron' for three-pulse ESEEM and HYSCORE and a home-written script involving EasySpin functions for EDNMR spectra.

For calculation of the spin Hamiltonians of the ^{55}Mn tetramer-single electron spin manifolds that describe the EPR and ^{55}Mn-ENDOR spectra, the electron Zeeman term was treated exactly. The ^{55}Mn hyperfine terms were treated using second order perturbation theory. ^{55}Mn nuclear quadrupole interactions (NQI) are not resolved in both the EPR and ENDOR spectra and thus omitted in their simulations. The ^{55}Mn nuclear Zeeman terms were not included in the EPR simulations (see sections S4.2 and S4.3). The G and the four effective ^{55}Mn hyperfine tensors A_i were assumed to be collinear. First-derivative X- and Q-band EPR, and absorption-line W-band EPR and Q-band ^{55}Mn-ENDOR data were simultaneously fit using a least squares routine.

For simulation of the (orientation-selective) ESEEM, HYSCORE and EDNMR spectra, ^{14}N, ^{15}N and ^{17}O single nucleus-single electron spin Hamiltonians were used. The ^{55}Mn nuclear interactions were not considered explicitly, but accounted for by employing hyperfine strain, *i.e.* an isotropic broadening due to unresolved hyperfine couplings, to compute the excitation window. All other spin Hamiltonian terms were treated exactly. In the simulations of the ^{17}O-EDNMR spectra, the NQI term was omitted as it is not resolved within the line width.

ESEEM simulation traces were fitted to the time-domain spectra. The X-band ESEEM spectra were fitted including two nitrogen nuclei and contributions from ^{1}H nuclei simulated by a hyperfine interaction A_i = [−0.44 −0.44 1.44] MHz.

EDNMR transition intensities were calculated assuming small angle excitation by the high turning angle (HTA) pulse, as described in Cox *et al.* [4]. As in Refs. [1, 5], the contributions from different nuclear species, as well as their individual single- and double-quantum transition envelopes, were calculated and normalized separately. Specifically, for the ^{17}O signal envelopes, which are made up of multiple species,

the fitting was constrained such that the relative intensities of the different contributions were scaled according to the magnitude of the anisotropic component of the hyperfine interaction.

S4 Theoretical background

S4.1 The spin Hamiltonian formalism. Here, we consider a single ligand ^{14}N, ^{15}N or ^{17}O nucleus magnetically interacting with an exchange-coupled Mn tetramer. The current assignment for the oxidation states of the four Mn ions when poised in the S_2 state is $Mn^{III}Mn^{IV}Mn^{IV}Mn^{IV}$.[6-13] This net oxidation state is assumed throughout the text. A basis set that describes the ^{14}N-, ^{15}N- or ^{17}O-Mn-tetramer spin manifold can be built from the product of the eigenstates of the interacting spins:

$$\left|S_1 S_2 S_3 S_4 M_1 M_2 M_3 M_4 I_1 I_2 I_3 I_4 m_1 m_2 m_3 m_4 L k\right\rangle, \qquad \text{(Eq. S1)}$$

Here, S_i (with i = 1 − 4) refers to the electronic spin state of Mn_i, M_i refers to the electronic magnetic sublevel of Mn_i, I_i refers to the nuclear spin state of Mn_i, and m_i refers to the nuclear magnetic sublevels of Mn_i. S_i takes the value 2 for Mn^{III} and 3/2 for Mn^{IV}; M_i takes the values: S_i, S_i-1, ..., 1-S_i, −S_i; I_i takes the value 5/2 for ^{55}Mn, m_i takes the values –I_i, 1-I_i, ..., I_i-1, I_i, L takes the values 1 for ^{14}N, ½ for ^{15}N and 5/2 for ^{17}O, and k takes the values –L, 1-L, ..., L-1, L.

The spin Hamiltonian that describes the spin manifold of the ^{14}N-, ^{15}N- or ^{17}O-Mn tetramer is:

$$H = \sum_i \beta_e \vec{B}_0 \cdot \hat{g}_i \cdot \vec{S}_i + \sum_i \vec{S}_i \cdot \hat{d}_i \cdot \vec{S}_i + \sum_{i<j} \vec{S}_i \cdot \hat{J}_{ij} \cdot \vec{S}_j - \sum_i g_{\mathrm{Mn}} \beta_n \vec{B}_0 \cdot \vec{I}_i + \sum_i \vec{S}_i \cdot \hat{a}_{\mathrm{Mn},i} \cdot \vec{I}_i$$
$$+ \sum_i \vec{I}_i \cdot \hat{q}_{\mathrm{Mn},i} \cdot \vec{I}_i - g_L \beta_n \vec{B}_0 \cdot \vec{L} + \vec{S}_L \cdot \hat{a}_L \cdot \vec{L} + \vec{L} \cdot q_L \cdot \vec{L} \qquad \text{(Eq. S2)}$$

It contains (i) an electronic Zeeman term for each Mn (g_i) ion, (ii) a fine structure term for each Mn (d_i) ion, and (iii) pair-wise electronic exchange terms for each Mn-Mn (J_{ij}) interaction, (iv) a nuclear Zeeman term for each ^{55}Mn (g_{Mn}) nucleus and the ligand (g_L) nucleus, (v) an electron-nuclear hyperfine term for each ^{55}Mn ($a_{\mathrm{Mn},i}$) nucleus and the ligand (a_L) nucleus (vi) an NQI term for each ^{55}Mn ($q_{\mathrm{Mn},i}$) and the ligand (q_L) nucleus.

S4.2 An effective spin S_T = ½ ground state. A basis set that describes the entire spin manifold of the coupled four ^{55}Mn ions of the OEC requires 414720 vectors, too many to be readily handled by current numerical techniques. The problem can be greatly simplified by assuming that all Mn-Mn couplings are large, *i.e.* within the strong exchange limit. For this to apply, the exchange interactions between the Mn ions have to be significantly larger than any other term of the spin Hamiltonian. The resultant electronic spin states of the manifold are then adequately described by a single quantum number, the total spin (S_T). The multiline EPR signal observed for the S_2 state of the OEC is derived from only one total spin state, the ground state of the spin manifold with total spin S_T = ½. The basis set that describes this subspace requires only 15552 vectors in the case that models the coupling of the effective electronic spin (S_T = ½) to the nuclear spin of each ^{55}Mn (I = 5/2) and a single ligand (L) nucleus:

$$\left|\tfrac{1}{2} \quad M \quad I_1 \quad I_2 \quad I_3 \quad I_4 \quad m_1 \quad m_2 \quad m_3 \quad m_4 \quad L \quad k\right\rangle \qquad \text{(Eq. S3)}$$

Where M takes all half-integer values $-\frac{1}{2} \le M \le \frac{1}{2}$, m_i takes all half-integer values $-\frac{5}{2} \le m_i \le \frac{5}{2}$, and k takes values $-L \le k \le L$.

The effective spin Hamiltonian that describes the ground state of the spin manifold (S_T = ½) is:

$$H = \beta_e \vec{B}_0 \cdot \hat{G} \cdot \vec{S} + \sum_i \left(- g_{Mn} \beta_n \vec{B}_0 \cdot \vec{I}_i + \vec{S} \cdot \hat{A}_{Mn,i} \cdot \vec{I}_i \right) - g_L \beta_n \vec{B}_0 \cdot \vec{L} + \vec{S}_L \cdot \hat{A}_L \cdot \vec{L} + \vec{L} \cdot q_L \cdot \vec{L} \qquad \text{(Eq. S4)}$$

It contains, (i) the Zeeman term for the total electronic spin, (ii) Zeeman terms for each ^{55}Mn and the ligand nucleus, (iii) hyperfine terms for each ^{55}Mn and the ligand nucleus and (iv) a quadrupole term for the ligand nucleus. Quadrupole terms are neglected for the ^{55}Mn nuclei as their size is smaller than the fitted line width.

S4.3 Application to the different spectroscopic experiments. The simulation of spectra from EPR and related experiments probing electronic spin transitions of the OEC can be further simplified. As the ligand couplings are comparatively small, they do not significantly contribute to the inhomogeneous line width of the S_2 state EPR spectrum. Thus, for simulation of the EPR spectrum, the terms in Eq. S4 relating to the ligand nucleus can be excluded (Eq. S5).

$$H_{\mathrm{EPR}} = \beta_{\mathrm{e}} \vec{B}_0 \cdot \hat{G} \cdot \vec{S} + \sum_i \vec{S} \cdot \hat{A}_{\mathrm{Mn},i} \cdot \vec{I}_i \qquad \text{(Eq. S5)}$$

Also, a simplified effective spin Hamiltonian can be used for the simulation of the spectra from experiments probing nuclear magnetic interactions, as the various nuclei do not significantly couple to each other. Thus, for the simulation of the ^{55}Mn-ENDOR resonances, terms in Eq. 4 associated with the ligand nucleus can be excluded:

$$H_{\mathrm{MnENDOR}} = \beta_{\mathrm{e}} \vec{B}_0 \cdot \hat{G} \cdot \vec{S} + \sum_i \left(- g_{\mathrm{Mn}} \beta_{\mathrm{n}} \vec{B}_0 \cdot \vec{I}_i + \vec{S} \cdot \hat{A}_{\mathrm{Mn},i} \cdot \vec{I}_i \right) \qquad \text{(Eq. S6)}$$

Similarly, for describing the nuclear interactions of a ligand ^{14}N, ^{15}N or ^{17}O nucleus in the various experiments (ESEEM, HYSCORE, EDNMR), the terms relating to the ^{55}Mn nuclei in Eq. 4 can be omitted:

$$H_{\mathrm{Ligand}} = \beta_{\mathrm{e}} \vec{B}_0 \cdot \hat{G} \cdot \vec{S} - g_{\mathrm{L}} \beta_{\mathrm{n}} \vec{B}_0 \cdot \vec{L} + \vec{S}_{\mathrm{L}} \cdot \hat{A}_{\mathrm{L}} \cdot \vec{L} + \vec{L} \cdot q_{\mathrm{L}} \cdot \vec{L} \qquad \text{(Eq. S7)}$$

In practice, however, the spin Hamiltonian in Eq. S7 is only valid when an ESEEM, ENDOR or EDNMR spectrum is collected at the center field of the S_2 state multiline spectrum as at this position all powder pattern orientations are sampled uniformly. Especially at W-band, spectra collected on the high- and low-field edges of the multiline spectrum must also take into account the sampling of the powder pattern orientations, which for the S_2 state ^{55}Mn tetramer is defined by the hyperfine coupling of the ^{55}Mn nuclei along with the *G* tensor. Eq. S7 can still be used (*i.e.*, terms associated with the ^{55}Mn nuclei can be excluded), but each orientation must include a weighting derived from simulation of the EPR line shape, for which the ^{55}Mn hyperfine interactions are taken account by hyperfine strain.

S5 DFT calculations: NH_3 binding modes and spatial coordinates of the S_2 state models

S5.1 Different coordination modes for the NH_3-annealed S_2 state and corresponding energies

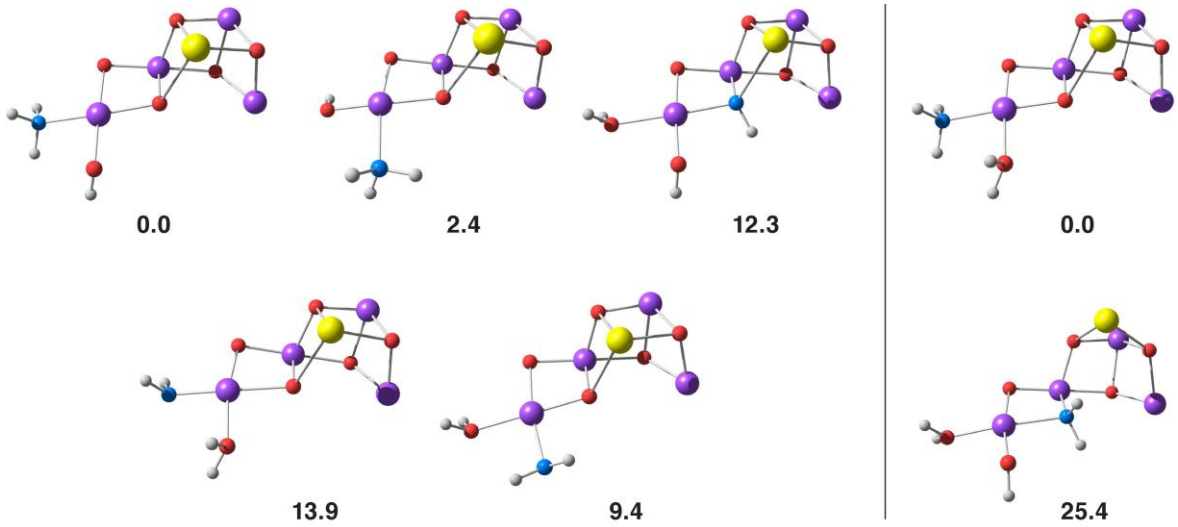

Fig. S2 Optimized structures (only the inorganic core framework and the terminal Mn_{A4} ligands are shown) and relative energies in kcal/mol of alternative models for NH_3, NH_2 and NH binding. The five structures on the left and the two structures on the right form two isomer sets. Although the complexity of the OEC structure and the extensive hydrogen bonding between terminal ligands and the surrounding residues and H_2O molecules make it difficult to isolate the structural origin of all energy differences, the results demonstrate unambiguously that terminal NH_3 coordination by W1 displacement (top left) is the energetically preferred interaction mode of ammonia with the OEC cluster.

S5.2 Cartesian coordinates of the optimized DFT structures

Mn_4O_5Ca

Mn	-24.848563	-35.523079	203.967881
Mn	-27.334886	-35.213752	205.224408
Mn	-27.324954	-33.347594	203.139609
Mn	-27.586920	-33.190450	200.400671
Ca	-27.866960	-36.744419	202.214036
O	-26.417337	-36.501815	204.230462
O	-28.351166	-34.735051	203.786382
O	-26.000441	-34.050081	204.476435
O	-28.501367	-32.618552	201.966909
O	-26.773447	-34.313956	201.661037
O	-28.452549	-31.704459	199.310367
O	-26.673182	-33.801897	198.916579
O	-27.535444	-37.283560	199.908060
O	-28.039762	-39.149284	202.493992
H	-30.449048	-26.810280	200.178402
C	-30.241434	-27.113395	201.222163
H	-30.724377	-26.361921	201.871645
C	-28.735963	-27.341748	201.414363
C	-28.199732	-28.497414	200.548849
O	-28.978095	-29.534053	200.450413
O	-27.065544	-28.401467	200.005515
C	-32.924381	-41.850903	196.489835
C	-31.571913	-41.351348	195.946748
C	-30.565368	-41.203392	197.075929
C	-30.005378	-42.352283	197.678852
C	-30.219133	-39.945803	197.617817
C	-29.142594	-42.263841	198.782163
C	-29.355473	-39.836453	198.721946
C	-28.815969	-40.996556	199.313115
O	-27.951563	-40.860113	200.380987
H	-33.785375	-32.318034	197.913159
C	-32.844739	-31.791422	197.688620
C	-31.633691	-32.698381	197.678058
O	-30.479771	-32.238554	197.548579
H	-32.684897	-30.983928	198.422799
N	-31.875152	-34.044975	197.757512
C	-30.825021	-35.049751	197.612821
C	-30.888736	-35.854848	196.310427
O	-30.009176	-36.709569	196.081062
C	-30.640197	-35.902739	198.882726
C	-29.824344	-35.261129	200.019523
O	-29.870659	-35.777979	201.169788
O	-29.067769	-34.275626	199.682792
N	-31.870257	-35.507945	195.452069
C	-31.935591	-35.967611	194.072817
H	-31.190723	-35.442656	193.449429
H	-21.516057	-41.187718	202.032943
C	-22.352883	-41.458335	202.717392
C	-22.781191	-42.906955	202.604719
O	-23.563034	-43.422685	203.424699
C	-23.549150	-40.504733	202.473898
C	-23.066676	-39.045303	202.457023
C	-24.154409	-37.985608	202.560664
O	-25.245648	-38.054524	201.948944
O	-23.811291	-36.982100	203.323874
N	-22.260513	-43.593061	201.547319
C	-22.629343	-44.962153	201.252063
H	-21.726399	-45.520632	200.924621
C	-23.730290	-45.086017	200.172457
C	-24.993767	-44.407864	200.583663
C	-25.537884	-43.184397	200.232720
N	-25.837688	-44.902174	201.568679
C	-26.833926	-44.005179	201.787416
N	-26.676843	-42.954433	200.984287
H	-19.262626	-31.517297	202.779917
C	-20.112713	-31.328697	202.090235
C	-21.154324	-30.545460	202.872811
O	-21.427294	-30.809815	204.064559
C	-20.718700	-32.621528	201.484318
C	-21.588166	-33.370625	202.438984
C	-22.935559	-33.687611	202.415622
N	-21.124735	-33.845842	203.657796
C	-22.142018	-34.418977	204.333486
N	-23.257629	-34.340485	203.596833
N	-21.804706	-29.583301	202.173241
C	-22.896307	-28.815019	202.759171
H	-22.557559	-28.453986	203.752878
C	-24.184294	-29.659284	202.927390
C	-24.721999	-30.234810	201.610409
C	-25.721730	-31.373018	201.743287
O	-26.013183	-31.839215	202.892913
O	-26.200648	-31.819686	200.639196
H	-24.820614	-28.955951	209.209804
C	-25.289739	-29.704836	209.874338
H	-25.215628	-29.314217	210.902923
C	-24.609120	-31.083522	209.710893
C	-24.555063	-31.562096	208.286908
C	-25.355784	-32.430055	207.562703
N	-23.592938	-31.124472	207.378052
C	-23.785244	-31.692405	206.168990
N	-24.861039	-32.482961	206.269039
H	-24.708982	-37.374838	210.156821
C	-25.333665	-37.110846	209.273415
C	-26.302066	-38.223140	208.875615
O	-26.045971	-39.056800	207.985385
C	-24.390518	-36.709013	208.141123
C	-24.995314	-36.021256	206.922435
O	-26.247447	-35.729512	206.899027
O	-24.176239	-35.777058	205.979846
N	-27.489289	-38.237933	209.552060
C	-28.420988	-39.357108	209.469748
C	-29.302576	-39.449882	208.216351
O	-29.919350	-40.500558	207.967913
N	-29.381138	-38.331183	207.462795
C	-30.071767	-38.285876	206.178140
C	-29.365555	-37.278820	205.263257
O	-29.557519	-37.302203	204.036093
O	-28.618993	-36.427231	205.917796
O	-25.189563	-37.830945	197.327508
O	-27.362976	-35.979546	197.623234
O	-26.499610	-30.205345	198.030232
O	-24.648447	-32.100460	198.143353
O	-29.820167	-30.416904	202.822043
O	-25.769334	-39.372428	199.682432
O	-26.808162	-39.050579	205.080655
H	-30.315328	-30.632298	208.999280
C	-30.997751	-31.051074	208.236197
H	-31.843803	-31.521736	208.767318
C	-30.280438	-32.094002	207.365998
C	-29.002550	-31.542167	206.704535
C	-28.324785	-32.556191	205.806489
O	-28.076520	-33.718646	206.300284
O	-28.029510	-32.191613	204.620538
H	-36.639768	-31.792575	206.865042
C	-36.971479	-32.276075	205.926511
C	-35.764944	-32.788933	205.115057
C	-34.832529	-33.697006	205.940910
C	-33.756434	-34.444822	205.142553
N	-32.759739	-33.538384	204.548528
C	-31.817337	-33.925669	203.659223
N	-31.645432	-35.231088	203.388681
N	-31.087087	-33.019146	202.995109
O	-27.626729	-29.307939	204.155135
H	-32.788273	-42.803281	197.036192
H	-33.336860	-41.123350	197.214330
H	-33.700323	-42.030393	195.723193
H	-31.702054	-40.382213	195.428906
H	-31.186938	-42.064851	195.191736
H	-30.251674	-43.345312	197.277293
H	-28.718529	-43.170884	199.228945
H	-29.068205	-38.858894	199.129846
H	-30.611394	-39.027180	197.158676
H	-27.492399	-41.807672	200.683751
H	-25.186432	-42.463282	199.492006
H	-27.637869	-44.150683	202.510626
H	-28.777126	-37.534390	207.680920
H	-27.643151	-37.538128	210.276277
H	-21.526504	-29.397911	201.211747
H	-21.667892	-43.094004	200.886496
H	-22.974272	-45.418365	202.196465
H	-23.906301	-46.160356	199.971989
H	-23.378923	-44.635507	199.227014
H	-22.513535	-38.839070	201.518066
H	-24.047081	-40.756192	201.518478
H	-21.977561	-41.306868	203.747367
H	-22.355106	-38.865609	203.281935

H	-24.301734	-40.652867	203.270025
H	-26.358938	-29.763781	209.603411
H	-26.220428	-33.025771	207.856890
H	-23.147269	-31.534392	205.291984
H	-23.684622	-33.524182	201.638740
H	-22.065252	-34.899474	205.308562
H	-19.698085	-30.721961	201.264657
H	-23.076603	-27.937895	202.115324
H	-29.896088	-34.453597	197.496858
H	-32.820024	-34.354703	197.987338
H	-32.925528	-31.321758	196.691941
H	-32.460763	-34.722495	195.722132
H	-30.793684	-28.056205	201.384572
H	-19.901235	-33.268438	201.113909
H	-21.333568	-32.360309	200.605086
H	-25.923588	-36.230796	209.594643
H	-29.975762	-39.276336	205.695988
C	-31.564156	-37.928824	206.319346
H	-32.056613	-37.947667	205.331092
H	-32.062519	-38.671730	206.964277
H	-31.683667	-36.929700	206.775884
H	-29.094151	-39.310299	210.342798
H	-27.858742	-40.306732	209.536504
H	-23.602073	-36.034103	208.523038
H	-23.863239	-37.598136	207.748470
H	-30.066168	-36.812345	198.617400
H	-31.604854	-36.250281	199.292797
H	-31.385034	-30.210658	207.631826
H	-30.012169	-32.979335	207.971720
H	-28.269901	-31.258293	207.487263
H	-30.964891	-32.463056	206.575770
H	-29.201153	-30.638741	206.102238
H	-28.146833	-26.437556	201.181531
H	-28.500420	-27.615428	202.462237
H	-25.144131	-31.845570	210.304896
H	-23.576835	-31.046545	210.107853
H	-25.292301	-33.078319	205.481826
H	-37.548238	-31.526089	205.357493
H	-35.195683	-31.924827	204.717232
H	-35.436315	-34.474000	206.447865
H	-33.241171	-35.157342	205.817396
H	-37.650410	-33.104948	206.199040
H	-36.124111	-33.349679	204.228833
H	-34.351902	-33.112827	206.752078
H	-32.865338	-32.538412	204.705951
H	-34.232131	-35.033777	204.332879
H	-31.176326	-32.010814	203.158206
H	-31.976367	-35.949226	204.024923
H	-30.185561	-33.276123	202.558204
H	-30.914049	-35.512208	202.722443
H	-23.963557	-30.489480	203.618139
H	-25.216470	-29.463496	200.987817
H	-24.964386	-29.042215	203.409363
H	-23.890613	-30.637385	200.996140
H	-20.181078	-33.721257	204.021679
H	-25.897909	-33.224088	198.636671
H	-29.229519	-31.978237	198.744838
H	-28.667106	-30.776279	199.810498
H	-29.746630	-29.955121	201.936280
H	-29.241466	-31.207596	202.619636
H	-27.124877	-30.143312	204.225955
H	-28.475420	-29.634975	203.745033
H	-32.944446	-35.777473	193.676544
H	-31.725742	-37.049193	194.029264
H	-26.526019	-39.991045	199.877758
H	-25.481143	-39.036931	200.581548
H	-27.666916	-39.512951	203.330178
H	-27.537049	-36.751815	199.051621
H	-28.150279	-35.989060	197.036010
H	-27.193430	-35.042548	197.983106
H	-25.915461	-37.162327	197.336238
H	-25.390599	-38.411921	198.098016
H	-28.026489	-39.851553	201.791278
H	-26.878137	-38.012918	199.728867
H	-24.159252	-32.008798	198.980640
H	-25.260919	-31.287325	198.135510
H	-27.198052	-30.860903	198.286344
H	-26.609590	-29.529442	198.767862
H	-26.711950	-39.118824	206.056089
H	-26.544572	-38.112857	204.868630
H	-25.708383	-45.772595	202.082114
H	-22.831876	-30.479081	207.591768

Mn_4O_5Sr

Mn	-24.847522	-35.543564	204.005634
Mn	-27.322350	-35.221215	205.230987
Mn	-27.301408	-33.360082	203.133939
Mn	-27.570266	-33.190878	200.392937
Sr	-27.773969	-36.800711	202.185621
O	-26.395326	-36.530518	204.290632
O	-28.321095	-34.754475	203.778882
O	-25.984947	-34.062982	204.480107
O	-28.486683	-32.638832	201.963392
O	-26.729380	-34.301589	201.650723
O	-28.449881	-31.709891	199.309648
O	-26.642620	-33.791854	198.911122
O	-27.542861	-37.310450	199.773045
O	-28.067271	-39.274216	202.556052
H	-30.439098	-26.804571	200.178143
C	-30.241434	-27.113395	201.222163
H	-30.724377	-26.361921	201.871645
C	-28.738557	-27.350408	201.425078
C	-28.201955	-28.501402	200.553636
O	-28.977496	-29.540167	200.454472
O	-27.070837	-28.399496	200.005085
C	-32.924381	-41.850903	196.489835
C	-31.566967	-41.374251	195.939213
C	-30.558975	-41.227474	197.066268
C	-29.993014	-42.376462	197.663037
C	-30.222136	-39.970778	197.615746
C	-29.130223	-42.288611	198.766457
C	-29.360164	-39.862043	198.720908
C	-28.811541	-41.021967	199.303372
O	-27.943455	-40.884295	200.368763
H	-33.785375	-32.318034	197.913159
C	-32.844739	-31.791422	197.688620
C	-31.634108	-32.699247	197.680281
O	-30.480148	-32.239400	197.550866
H	-32.683822	-30.983826	198.422430
N	-31.875544	-34.045737	197.760638
C	-30.825021	-35.049751	197.612821
C	-30.891053	-35.854242	196.309656
O	-30.013559	-36.709922	196.077987
C	-30.630723	-35.903544	198.879125
C	-29.814141	-35.259888	200.014235
O	-29.875467	-35.762381	201.168485
O	-29.036385	-34.291453	199.668418
N	-31.872723	-35.506021	195.451452
C	-31.935591	-35.967611	194.072817
H	-31.190723	-35.442656	193.449429
H	-21.516057	-41.187718	202.032943
C	-22.352883	-41.458335	202.717392
C	-22.777025	-42.908578	202.607857
O	-23.549134	-43.427645	203.434844
C	-23.557907	-40.511524	202.471638
C	-23.084493	-39.047997	202.402297
C	-24.168388	-37.987059	202.549207
O	-25.264811	-38.035469	201.936834
O	-23.824841	-37.010368	203.340884
N	-22.265032	-43.591309	201.543887
C	-22.629343	-44.962153	201.252063
H	-21.726399	-45.520632	200.924621
C	-23.729143	-45.095444	200.172928
C	-24.996925	-44.427297	200.585019
C	-25.548238	-43.206738	200.236361
N	-25.836503	-44.927692	201.570687
C	-26.838027	-44.036674	201.791173
N	-26.687631	-42.984336	200.989178
H	-19.262626	-31.517297	202.779917
C	-20.112713	-31.328697	202.090235
C	-21.148504	-30.538340	202.872859
O	-21.414636	-30.796357	204.067668
C	-20.734300	-32.622151	201.497733
C	-21.603451	-33.368201	202.457635
C	-22.946290	-33.707963	202.429191
N	-21.137532	-33.838032	203.677440
C	-22.148150	-34.428194	204.348756
N	-23.262770	-34.367262	203.608879
N	-21.803538	-29.580554	202.172049
C	-22.896307	-28.815019	202.759171
H	-22.557559	-28.453986	203.752878
C	-24.181716	-29.660126	202.928755
C	-24.722407	-30.227121	201.610337
C	-25.718949	-31.367117	201.740658

O	-26.002379	-31.842055	202.889037
O	-26.202553	-31.805270	200.635606
H	-24.809359	-28.960819	209.212244
C	-25.289739	-29.704836	209.874338
H	-25.215628	-29.314217	210.902923
C	-24.624893	-31.091091	209.712480
C	-24.560543	-31.562523	208.286764
C	-25.349798	-32.434305	207.554921
N	-23.595543	-31.114786	207.385870
C	-23.774996	-31.680275	206.174006
N	-24.844970	-32.480241	206.264675
H	-24.708982	-37.374838	210.156821
C	-25.333665	-37.110846	209.273415
C	-26.300933	-38.224773	208.878926
O	-26.040335	-39.063990	207.994690
C	-24.386912	-36.712850	208.142561
C	-24.992459	-36.022343	206.927704
O	-26.238003	-35.710160	206.916372
O	-24.180164	-35.793742	205.972439
N	-27.489437	-38.237473	209.551622
C	-28.420988	-39.357108	209.469748
C	-29.305038	-39.447628	208.219771
O	-29.913924	-40.500987	207.963740
N	-29.398341	-38.320876	207.480263
C	-30.085454	-38.273385	206.194923
C	-29.369811	-37.276449	205.276851
O	-29.564530	-37.306122	204.050969
O	-28.612781	-36.428849	205.927101
O	-25.151856	-37.834078	197.301915
O	-27.316256	-35.932702	197.549365
O	-26.508973	-30.194245	198.024114
O	-24.637913	-32.066365	198.138137
O	-29.799381	-30.430228	202.827438
O	-25.767207	-39.391760	199.664435
O	-26.825769	-39.097706	205.138143
H	-30.315733	-30.628829	208.997803
C	-30.997751	-31.051074	208.236197
H	-31.843803	-31.521736	208.767318
C	-30.279499	-32.096912	207.368279
C	-29.013025	-31.545151	206.684315
C	-28.327552	-32.563676	205.795194
O	-28.080955	-33.723607	206.294970
O	-28.019919	-32.203459	204.611063
H	-36.640291	-31.793756	206.865827
C	-36.971479	-32.276075	205.926511
C	-35.763832	-32.788497	205.115190
C	-34.833474	-33.699931	205.939590
C	-33.756307	-34.446956	205.141711
N	-32.752267	-33.542214	204.556972
C	-31.804334	-33.931414	203.673704
N	-31.636098	-35.237271	203.401154
N	-31.063395	-33.027386	203.019445
O	-27.601196	-29.322117	204.155150
H	-32.799026	-42.798213	197.047485
H	-33.328280	-41.109535	197.204990
H	-33.700323	-42.030393	195.723193
H	-31.686363	-40.408931	195.411657
H	-31.191800	-42.100324	195.191443
H	-30.234818	-43.368675	197.256731
H	-28.698804	-43.195183	199.207076
H	-29.076401	-38.884424	199.130778
H	-30.622065	-39.052237	197.162989
H	-27.496965	-41.832812	200.676915
H	-25.201723	-42.482824	199.495993
H	-27.640563	-44.188034	202.514743
H	-28.796871	-37.523202	207.702171
H	-27.646985	-37.533196	210.270738
H	-21.530663	-29.399200	201.208242
H	-21.677238	-43.090484	200.880086
H	-22.972298	-45.416804	202.197911
H	-23.896325	-46.171435	199.973817
H	-23.381788	-44.643190	199.226835
H	-22.586096	-38.858679	201.430002
H	-24.075507	-40.790807	201.534579
H	-21.978856	-41.301263	203.746797
H	-22.329213	-38.853074	203.183342
H	-24.292487	-40.641882	203.287421
H	-26.358163	-29.750767	209.597917
H	-26.212428	-33.037018	207.840907
H	-23.131951	-31.515173	205.301802
H	-23.694957	-33.556265	201.649320
H	-22.064848	-34.903542	205.325894
H	-19.698989	-30.731536	201.257490
H	-23.078141	-27.937489	202.116223
H	-29.897362	-34.451898	197.493798
H	-32.820543	-34.355979	197.989244
H	-32.924671	-31.323090	196.691292
H	-32.462081	-34.719217	195.719947
H	-30.799119	-28.054470	201.376360
H	-19.923868	-33.276165	201.124087
H	-21.352685	-32.360734	200.620986
H	-25.922558	-36.229605	209.592752
H	-29.994641	-39.266225	205.716684
C	-31.576011	-37.907338	206.331053
H	-32.067356	-37.932300	205.342274
H	-32.079669	-38.642684	206.980616
H	-31.691811	-36.904409	206.780181
H	-29.091703	-39.310203	210.344813
H	-27.858742	-40.306732	209.536504
H	-23.596107	-36.041001	208.525313
H	-23.862657	-37.603793	207.749980
H	-30.050373	-36.807660	198.607772
H	-31.591393	-36.257878	199.292352
H	-31.385678	-30.212245	207.629892
H	-29.997571	-32.973704	207.980342
H	-28.275550	-31.242364	207.455690
H	-30.970870	-32.481000	206.591322
H	-29.225496	-30.652409	206.071063
H	-28.143299	-26.447157	201.204788
H	-28.515263	-27.633724	202.472907
H	-25.176840	-31.849150	210.295893
H	-23.596685	-31.069489	210.121075
H	-25.263958	-33.079645	205.475862
H	-37.548238	-31.526089	205.357493
H	-35.192968	-31.924153	204.720225
H	-35.439101	-34.477597	206.443308
H	-33.246866	-35.164547	205.815492
H	-37.650169	-33.105545	206.197916
H	-36.123233	-33.346500	204.227348
H	-34.353989	-33.118344	206.753344
H	-32.855061	-32.542337	204.716747
H	-34.229824	-35.030561	204.326920
H	-31.151166	-32.017954	203.176466
H	-31.961562	-35.953099	204.042903
H	-30.166465	-33.291444	202.577663
H	-30.904473	-35.519002	202.735048
H	-23.957359	-30.494506	203.613336
H	-25.219372	-29.452700	200.993647
H	-24.960906	-29.046996	203.417023
H	-23.892524	-30.625725	200.991398
H	-20.197134	-33.699832	204.044862
H	-25.877474	-33.200854	198.630977
H	-29.228123	-31.984420	198.745683
H	-28.665148	-30.783519	199.810884
H	-29.730725	-29.966661	201.941859
H	-29.223680	-31.221872	202.621833
H	-27.099379	-30.157492	204.225445
H	-28.451184	-29.648882	203.747647
H	-32.944167	-35.779525	193.674748
H	-31.724175	-37.048948	194.031317
H	-26.524888	-40.007743	199.869361
H	-25.495558	-39.036622	200.559927
H	-27.694527	-39.630438	203.395105
H	-27.524991	-36.745460	198.935755
H	-28.113528	-35.928027	196.976887
H	-27.152045	-35.006961	197.941725
H	-25.869508	-37.157570	197.302270
H	-25.364133	-38.418680	198.065646
H	-28.051327	-39.973546	201.850653
H	-26.872156	-38.027902	199.595628
H	-24.148642	-31.969282	198.974769
H	-25.258600	-31.259100	198.130512
H	-27.201408	-30.855776	198.280424
H	-26.621270	-29.520602	198.763778
H	-26.729391	-39.161847	206.114547
H	-26.556287	-38.163670	204.926956
H	-25.702708	-45.799042	202.081429
H	-22.841190	-30.463954	207.606809

Mn_4O_5Ca–NH_3

Mn	-24.864710	-35.521490	203.948726
Mn	-27.347645	-35.219577	205.222273
Mn	-27.313570	-33.383873	203.115499
Mn	-27.485767	-33.299034	200.363131
Ca	-27.838367	-36.773504	202.206296
O	-26.419856	-36.511777	204.238424
O	-28.356161	-34.755712	203.776060
O	-26.010801	-34.055338	204.486200
O	-28.448732	-32.678016	201.884329
O	-26.703765	-34.406807	201.716902
N	-28.266943	-31.835150	199.178604
O	-26.543687	-33.978771	198.919068
O	-27.544064	-37.346947	199.899022
O	-28.049725	-39.175016	202.519122
H	-30.509875	-26.860957	200.179093
C	-30.241434	-27.113395	201.222163
H	-30.724377	-26.361921	201.871645
C	-28.717362	-27.230848	201.366941
C	-28.147217	-28.372668	200.506754
O	-28.870316	-29.423316	200.397733
O	-27.003468	-28.225793	199.960457
C	-32.924381	-41.850903	196.489835
C	-31.581764	-41.318185	195.953559
C	-30.575680	-41.184853	197.084755
C	-29.977795	-42.339072	197.638888
C	-30.272636	-39.941171	197.681704
C	-29.119791	-42.269259	198.747269
C	-29.417002	-39.850281	198.793484
C	-28.839295	-41.016158	199.335137
O	-27.983212	-40.897097	200.411499
H	-33.785375	-32.318034	197.913159
C	-32.844739	-31.791422	197.688620
C	-31.653286	-32.714935	197.543999
O	-30.531221	-32.285140	197.217641
H	-32.633097	-31.060938	198.489041
N	-31.878803	-34.052802	197.766510
C	-30.825021	-35.049751	197.612821
C	-30.865287	-35.835399	196.298584
O	-29.945790	-36.642644	196.044494
C	-30.640852	-35.918810	198.872564
C	-29.789680	-35.310628	200.005116
O	-29.858555	-35.815521	201.157932
O	-28.981276	-34.372779	199.649010
N	-31.868631	-35.521649	195.456113
C	-31.935591	-35.967611	194.072817
H	-31.190723	-35.442656	193.449429
H	-21.516057	-41.187718	202.032943
C	-22.352883	-41.458335	202.717392
C	-22.776249	-42.908782	202.608354
O	-23.551661	-43.427050	203.432828
C	-23.552784	-40.510643	202.469132
C	-23.078230	-39.048869	202.449119
C	-24.171642	-37.994255	202.549317
O	-25.270984	-38.083792	201.953885
O	-23.825599	-36.975682	203.289600
N	-22.262672	-43.592225	201.545640
C	-22.629343	-44.962153	201.252063
H	-21.726399	-45.520632	200.924621
C	-23.731479	-45.089627	200.174408
C	-25.000266	-44.424899	200.591243
C	-25.559161	-43.206908	200.244674
N	-25.837340	-44.932188	201.575658
C	-26.844140	-44.047669	201.797756
N	-26.700283	-42.992700	200.997890
H	-19.262626	-31.517297	202.779917
C	-20.112713	-31.328697	202.090235
C	-21.149552	-30.539290	202.873280
O	-21.419003	-30.799420	204.066784
C	-20.723298	-32.618867	201.484204
C	-21.599273	-33.363171	202.436715
C	-22.944254	-33.689736	202.401952
N	-21.145202	-33.824906	203.664228
C	-22.166165	-34.398156	204.334587
N	-23.274161	-34.333814	203.585587
N	-21.799095	-29.576638	202.173515
C	-22.896307	-28.815019	202.759171
H	-22.557559	-28.453986	203.752878
C	-24.176837	-29.674212	202.924814
C	-24.722648	-30.242942	201.605811
C	-25.673598	-31.425442	201.731344
O	-26.018756	-31.851735	202.879987
O	-26.065736	-31.942535	200.620999
H	-24.801515	-28.965028	209.213262
C	-25.289739	-29.704836	209.874338
H	-25.215628	-29.314217	210.902923
C	-24.636080	-31.096445	209.714297
C	-24.578059	-31.571248	208.289346
C	-25.376593	-32.437107	207.560279
N	-23.611024	-31.133702	207.385609
C	-23.798680	-31.700932	206.175302
N	-24.875693	-32.490146	206.269295
H	-24.708982	-37.374838	210.156821
C	-25.333665	-37.110846	209.273415
C	-26.300738	-38.224866	208.877256
O	-26.041287	-39.063182	207.992233
C	-24.393954	-36.706939	208.139308
C	-25.002102	-36.019488	206.920698
O	-26.255457	-35.728630	206.900664
O	-24.183671	-35.775666	205.978534
N	-27.490167	-38.237322	209.549699
C	-28.420988	-39.357108	209.469748
C	-29.304581	-39.454352	208.217565
O	-29.921032	-40.506669	207.974643
N	-29.384204	-38.339404	207.458988
C	-30.071968	-38.300480	206.172216
C	-29.369738	-37.289425	205.258738
O	-29.561109	-37.312856	204.031272
O	-28.631097	-36.432971	205.915409
O	-25.256753	-37.985027	197.283490
O	-27.394488	-36.098233	197.572737
O	-26.252701	-29.970572	198.146402
O	-24.619668	-32.110776	198.117885
O	-29.701492	-30.390722	202.699176
O	-25.776766	-39.443943	199.703356
O	-26.817106	-39.052364	205.097592
H	-30.304360	-30.649272	208.998605
C	-30.997751	-31.051074	208.236197
H	-31.843803	-31.521736	208.767318
C	-30.299242	-32.089135	207.343432
C	-29.032035	-31.540173	206.658983
C	-28.353578	-32.561403	205.766910
O	-28.097633	-33.716666	206.279018
O	-28.062835	-32.210782	204.577261
H	-36.663406	-31.800759	206.877175
C	-36.971479	-32.276075	205.926511
C	-35.741686	-32.750576	205.123250
C	-34.772092	-33.611907	205.957189
C	-33.683948	-34.348734	205.163635
N	-32.719724	-33.434895	204.528030
C	-31.757597	-33.834930	203.664614
N	-31.543259	-35.145308	203.457803
N	-31.047224	-32.940683	202.962512
O	-27.559854	-29.319219	204.115328
H	-32.769260	-42.810763	197.017851
H	-33.346737	-41.144690	197.229596
H	-33.700323	-42.030393	195.723193
H	-31.728017	-40.338448	195.460444
H	-31.188644	-42.007082	195.180287
H	-30.190114	-43.321384	197.193914
H	-28.664658	-43.179784	199.154699
H	-29.160345	-38.882656	199.243123
H	-30.698698	-39.019225	197.260996
H	-27.525101	-41.846717	200.701984
H	-25.216575	-42.478730	199.506654
H	-27.645591	-44.204989	202.521261
H	-28.778547	-37.542060	207.671113
H	-27.647817	-37.533001	210.268672
H	-21.528970	-29.399498	201.208202
H	-21.676553	-43.090833	200.880790
H	-22.972246	-45.417617	202.197588
H	-23.899004	-46.164471	199.969225
H	-23.385908	-44.631971	199.230247
H	-22.524127	-38.841811	201.510847
H	-24.048025	-40.767550	201.513805
H	-21.979358	-41.302339	203.747290
H	-22.368586	-38.862857	203.274418
H	-24.306083	-40.660102	203.264364
H	-26.357875	-29.742211	209.595398
H	-26.245354	-33.029860	207.848221
H	-23.157158	-31.543306	205.301225
H	-23.687705	-33.541102	201.616471
H	-22.097321	-34.868618	205.315170
H	-19.696150	-30.723618	201.264263

H	-23.082995	-27.938595	202.116242
H	-29.896528	-34.451444	197.506025
H	-32.788477	-34.346718	198.122451
H	-32.960763	-31.226009	196.747974
H	-32.508765	-34.789033	195.760399
H	-30.726095	-28.079307	201.446514
H	-19.907851	-33.269977	201.116471
H	-21.334421	-32.355232	200.603054
H	-25.924836	-36.232018	209.595770
H	-29.968921	-39.290797	205.691356
C	-31.566606	-37.950180	206.306780
H	-32.053587	-37.969970	205.315712
H	-32.065376	-38.694688	206.949586
H	-31.692411	-36.951538	206.763000
H	-29.093141	-39.309782	210.343565
H	-27.858742	-40.306732	209.536504
H	-23.606290	-36.030492	208.520086
H	-23.865768	-37.595129	207.745866
H	-30.091398	-36.837912	198.589096
H	-31.606074	-36.249832	199.294797
H	-31.383088	-30.198805	207.647171
H	-30.022455	-32.978919	207.938924
H	-28.291208	-31.242267	207.429080
H	-31.000414	-32.449630	206.564168
H	-29.241508	-30.645701	206.047098
H	-28.201164	-26.291361	201.100794
H	-28.433679	-27.467158	202.412584
H	-25.192552	-31.849316	210.300155
H	-23.607107	-31.081871	210.121448
H	-25.301826	-33.092668	205.481387
H	-37.548238	-31.526089	205.357493
H	-35.206812	-31.867903	204.718424
H	-35.346282	-34.395013	206.488669
H	-33.137664	-35.023617	205.852756
H	-37.638922	-33.121520	206.174438
H	-36.077468	-33.332731	204.241646
H	-34.299288	-32.994667	206.747906
H	-32.881960	-32.433240	204.607462
H	-34.154886	-34.977513	204.381055
H	-31.127673	-31.930556	203.116276
H	-31.894146	-35.848399	204.099494
H	-30.148132	-33.204508	202.521251
H	-30.781219	-35.435485	202.834111
H	-23.940373	-30.509478	203.604410
H	-25.272365	-29.475630	201.023353
H	-24.960097	-29.072100	203.419980
H	-23.895851	-30.584811	200.951486
H	-20.207291	-33.687520	204.038040
H	-25.850528	-33.350448	198.562721
H	-29.051411	-32.169779	198.597391
H	-28.561419	-30.986686	199.723501
H	-29.591533	-29.909901	201.820146
H	-29.150648	-31.199882	202.502410
H	-27.071636	-30.162627	204.186895
H	-28.390706	-29.627465	203.654027
H	-32.944161	-35.768869	193.680452
H	-31.732285	-37.050323	194.016067
H	-26.538760	-40.048751	199.918316
H	-25.486437	-39.080015	200.590800
H	-27.678024	-39.530650	203.359394
H	-27.556708	-36.833499	199.032423
H	-28.208271	-36.093374	197.015818
H	-27.192198	-35.172672	197.931551
H	-25.976613	-37.309574	197.292913
H	-25.433830	-38.534189	198.082737
H	-28.042027	-39.884749	201.824854
H	-26.893567	-38.081659	199.722400
H	-24.238397	-32.158521	199.013738
H	-25.182206	-31.277130	198.165728
H	-27.534839	-31.466199	198.547559
H	-26.560745	-29.326508	198.890050
H	-26.714168	-39.115546	206.072735
H	-26.543578	-38.118929	204.876642
H	-25.698492	-45.803642	202.084843
H	-22.850254	-30.489410	207.603340
H	-26.357141	-29.474536	197.313611

Mn_4O_5Sr–NH_3

Mn	-24.870509	-35.539329	203.989923
Mn	-27.340841	-35.222259	205.228375
Mn	-27.292163	-33.392297	203.110512
Mn	-27.476682	-33.295887	200.355604
Sr	-27.752982	-36.822127	202.179576
O	-26.406325	-36.535667	204.295951
O	-28.332329	-34.768821	203.768907
O	-26.001418	-34.064573	204.491932
O	-28.436041	-32.690994	201.881801
O	-26.663437	-34.389934	201.707436
N	-28.270236	-31.836664	199.173019
O	-26.530811	-33.968438	198.908871
O	-27.559152	-37.383758	199.770505
O	-28.082822	-39.294418	202.579115
H	-30.511930	-26.862077	200.179348
C	-30.241434	-27.113395	201.222163
H	-30.724377	-26.361921	201.871645
C	-28.716820	-27.229948	201.363685
C	-28.147090	-28.369839	200.500231
O	-28.870145	-29.420590	200.389066
O	-27.003767	-28.221983	199.953847
C	-32.924381	-41.850903	196.489835
C	-31.591286	-41.295157	195.953669
C	-30.580898	-41.171873	197.081378
C	-29.937040	-42.324334	197.584858
C	-30.322810	-39.943417	197.728551
C	-29.074501	-42.266780	198.690600
C	-29.465369	-39.865292	198.839427
C	-28.838579	-41.028995	199.328269
O	-27.975519	-40.919512	200.400304
H	-33.785375	-32.318034	197.913159
C	-32.844739	-31.791422	197.688620
C	-31.655305	-32.717606	197.543642
O	-30.533492	-32.289763	197.213592
H	-32.632048	-31.061552	198.489283
N	-31.880706	-34.055156	197.770125
C	-30.825021	-35.049751	197.612821
C	-30.858404	-35.825563	196.292943
O	-29.923667	-36.611134	196.026084
C	-30.631803	-35.922702	198.866495
C	-29.786836	-35.308747	200.001542
O	-29.874668	-35.798116	201.157354
O	-28.960611	-34.385092	199.639541
N	-31.870492	-35.524436	195.456880
C	-31.935591	-35.967611	194.072817
H	-31.190723	-35.442656	193.449429
H	-21.516057	-41.187718	202.032943
C	-22.352883	-41.458335	202.717392
C	-22.774231	-42.909619	202.609580
O	-23.543294	-43.430115	203.438550
C	-23.558783	-40.515366	202.468346
C	-23.092230	-39.049970	202.420715
C	-24.186159	-37.997152	202.545792
O	-25.286445	-38.077515	201.942668
O	-23.847022	-36.996896	203.307240
N	-22.266811	-43.590684	201.542341
C	-22.629343	-44.962153	201.252063
H	-21.726399	-45.520632	200.924621
C	-23.728796	-45.098880	200.173284
C	-25.002428	-44.443408	200.587577
C	-25.567040	-43.228574	200.240535
N	-25.837911	-44.955603	201.570800
C	-26.850857	-44.077366	201.790468
N	-26.711062	-43.021754	200.990983
H	-19.262626	-31.517297	202.779917
C	-20.112713	-31.328697	202.090235
C	-21.142051	-30.529960	202.873739
O	-21.404472	-30.782789	204.070537
C	-20.743469	-32.618576	201.499916
C	-21.620941	-33.357372	202.458280
C	-22.961443	-33.706184	202.418193
N	-21.165378	-33.813624	203.687212
C	-22.180107	-34.404189	204.352655
N	-23.286237	-34.357118	203.599989
N	-21.797752	-29.573286	202.171792
C	-22.896307	-28.815019	202.759171
H	-22.557559	-28.453986	203.752878
C	-24.173579	-29.676573	202.925769
C	-24.726314	-30.232580	201.605000
C	-25.672560	-31.418409	201.727008

O	-26.007616	-31.854330	202.875286
O	-26.070516	-31.926253	200.614765
H	-24.800910	-28.965208	209.213497
C	-25.289739	-29.704836	209.874338
H	-25.215628	-29.314217	210.902923
C	-24.636445	-31.096368	209.714303
C	-24.576420	-31.568127	208.288617
C	-25.374814	-32.430712	207.555672
N	-23.608563	-31.127262	207.387445
C	-23.793881	-31.690942	206.175362
N	-24.871308	-32.480384	206.265462
H	-24.708982	-37.374838	210.156821
C	-25.333665	-37.110846	209.273415
C	-26.298825	-38.227273	208.880875
O	-26.034080	-39.071731	208.002795
C	-24.393359	-36.707916	208.138466
C	-25.006546	-36.019809	206.923738
O	-26.253416	-35.709714	206.918387
O	-24.198206	-35.792488	205.965740
N	-27.490164	-38.237102	209.548700
C	-28.420988	-39.357108	209.469748
C	-29.308363	-39.451177	208.221618
O	-29.920824	-40.504489	207.973385
N	-29.400647	-38.328308	207.476552
C	-30.089803	-38.284032	206.191723
C	-29.377355	-37.284825	205.273604
O	-29.567899	-37.318561	204.046801
O	-28.632910	-36.427974	205.925130
O	-25.228282	-37.982119	197.252603
O	-27.361477	-36.060418	197.497938
O	-26.258547	-29.970485	198.136556
O	-24.600782	-32.092006	198.129105
O	-29.683302	-30.396811	202.691263
O	-25.777111	-39.465538	199.678778
O	-26.856479	-39.088755	205.162419
H	-30.302318	-30.651418	208.997851
C	-30.997751	-31.051074	208.236197
H	-31.843803	-31.521736	208.767318
C	-30.302753	-32.089436	207.339341
C	-29.042886	-31.540018	206.641231
C	-28.356810	-32.563938	205.756527
O	-28.102777	-33.717484	206.273217
O	-28.053840	-32.216833	204.569059
H	-36.671474	-31.802446	206.880663
C	-36.971479	-32.276075	205.926511
C	-35.734039	-32.742129	205.130412
C	-34.759290	-33.588323	205.973971
C	-33.666355	-34.326064	205.188288
N	-32.712478	-33.412744	204.537143
C	-31.736449	-33.821997	203.692888
N	-31.499991	-35.132709	203.523249
N	-31.029268	-32.935795	202.977734
O	-27.549622	-29.324547	204.113995
H	-32.754117	-42.815413	197.004591
H	-33.352280	-41.159588	197.240309
H	-33.700323	-42.030393	195.723193
H	-31.751372	-40.308558	195.478760
H	-31.195976	-41.966346	195.166283
H	-30.116214	-43.295029	197.101498
H	-28.579777	-43.174588	199.055748
H	-29.240217	-38.906858	199.323388
H	-30.788422	-39.023181	197.348285
H	-27.526386	-41.873942	200.688637
H	-25.226807	-42.497666	199.504098
H	-27.653126	-44.239576	202.511964
H	-28.794171	-37.532057	207.690460
H	-27.651806	-37.527846	210.261959
H	-21.534419	-29.401559	201.203616
H	-21.682603	-43.088648	200.876292
H	-22.971258	-45.416172	202.198599
H	-23.887777	-46.175282	199.969547
H	-23.385288	-44.640150	199.228886
H	-22.568865	-38.850613	201.463442
H	-24.064555	-40.787839	201.522850
H	-21.980193	-41.299354	203.747011
H	-22.359002	-38.854140	203.222528
H	-24.301835	-40.657508	203.274482
H	-26.357774	-29.741578	209.595036
H	-26.245096	-33.023157	207.839884
H	-23.151367	-31.529694	205.302659
H	-23.704583	-33.568333	201.630201
H	-22.105384	-34.870781	205.334646
H	-19.697250	-30.734625	201.256062
H	-23.085872	-27.938089	202.117665
H	-29.899221	-34.446364	197.508854
H	-32.788640	-34.349051	198.130461
H	-32.960159	-31.226065	196.747923
H	-32.523787	-34.806491	195.767831
H	-30.724448	-28.079858	201.447803
H	-19.937574	-33.279712	201.128633
H	-21.357895	-32.353404	200.621460
H	-25.924889	-36.231881	209.594840
H	-29.998700	-39.276550	205.713370
C	-31.579953	-37.916363	206.329213
H	-32.070147	-37.933457	205.339639
H	-32.085942	-38.653299	206.975163
H	-31.693250	-36.915262	206.783374
H	-29.090655	-39.309697	210.345652
H	-27.858742	-40.306732	209.536504
H	-23.605484	-36.031269	208.518876
H	-23.865326	-37.595870	207.744462
H	-30.070251	-36.832955	198.577586
H	-31.592955	-36.265769	199.287937
H	-31.383226	-30.197413	207.649203
H	-30.018359	-32.976667	207.935066
H	-28.299911	-31.227380	207.403633
H	-31.010014	-32.453694	206.567346
H	-29.261543	-30.653567	206.020910
H	-28.202025	-26.289602	201.097828
H	-28.431085	-27.467010	202.408612
H	-25.194296	-31.849900	210.297998
H	-23.608113	-31.082826	210.123077
H	-25.294782	-33.083804	205.478370
H	-37.548238	-31.526089	205.357493
H	-35.206991	-31.855823	204.723199
H	-35.328758	-34.369673	206.513045
H	-33.110723	-34.984187	205.885955
H	-37.636458	-33.125324	206.167805
H	-36.059929	-33.332342	204.250509
H	-34.291166	-32.959631	206.758337
H	-32.905350	-32.413718	204.569143
H	-34.134988	-34.971931	204.417980
H	-31.102868	-31.924680	203.127769
H	-31.883470	-35.831315	204.150365
H	-30.134069	-33.206742	202.533270
H	-30.719044	-35.428700	202.928366
H	-23.931230	-30.518094	203.595585
H	-25.282088	-29.461133	201.033746
H	-24.954717	-29.080727	203.431699
H	-23.903268	-30.565599	200.941418
H	-20.231362	-33.661954	204.065249
H	-25.833108	-33.341442	198.560188
H	-29.057201	-32.174546	198.597216
H	-28.561046	-30.985814	199.716156
H	-29.577497	-29.914867	201.812199
H	-29.133717	-31.206666	202.492959
H	-27.065176	-30.169600	204.191299
H	-28.378077	-29.631591	203.647289
H	-32.943857	-35.767843	193.680253
H	-31.733037	-37.050448	194.013505
H	-26.540648	-40.065914	199.905515
H	-25.491279	-39.084972	200.559008
H	-27.702034	-39.639150	203.419397
H	-27.551924	-36.843399	198.918497
H	-28.191208	-36.056123	196.964152
H	-27.174080	-35.146680	197.893762
H	-25.944154	-37.303079	197.254847
H	-25.414702	-38.536933	198.044855
H	-28.058535	-39.999244	201.880339
H	-26.908205	-38.117800	199.592769
H	-24.237337	-32.138510	199.032375
H	-25.173977	-31.264988	198.168586
H	-27.541448	-31.471562	198.536193
H	-26.558768	-29.329519	198.885066
H	-26.729472	-39.161264	206.134768
H	-26.569953	-38.160553	204.945723
H	-25.695765	-45.827136	202.078993
H	-22.848922	-30.482577	207.608098
H	-26.345265	-29.460304	197.310298

S6 Q-band ^{55}Mn-ENDOR: comparison of instrumental settings

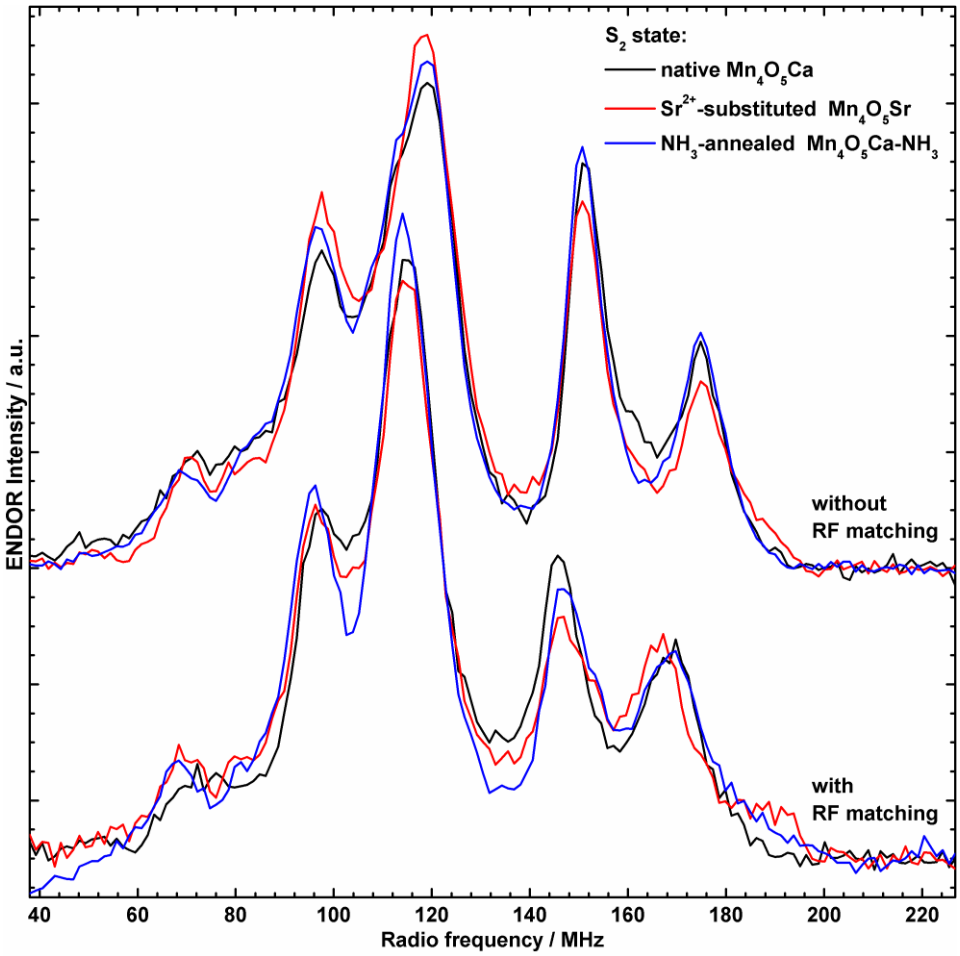

Fig. S3 Comparison of Q-band ^{55}Mn-ENDOR spectra of PSII samples isolated from *T. elongatus* in the native (Mn_4O_5Ca, black), Sr^{2+}-substituted (Mn_4O_5Ca, red) and NH_3-annealed (Mn_4O_5Ca–NH_3, blue) S_2 states recorded without (top traces) and with (bottom traces)[5] radio frequency (RF) matching employed. Shown are the spectra of illuminated samples without light-minus-dark subtraction. Experimental parameters: microwave frequencies: 33.9678 GHz (top, black), 33.9950 GHz (top, red), 34.0053 GHz (top, blue), 34.0368 GHz (bottom, black), 34.0435 GHz (bottom, red), 34.0159 GHz (bottom, blue); magnetic field: 1220 mT; shot repetition time: 1 ms; microwave pulse length (π): 32 ns (top), 24 ns (bottom); τ: 268 ns; RF pulse length (π_{RF}): 3.5 µs; temperature: 4.8 K (top), 5.2 K (bottom).

In order to overcome variations of the spectral shape, especially at higher frequencies (>150 MHz), the ^{55}Mn-ENDOR experiments presented here were performed under instrumental settings that allowed for the best reproducibility. To obtain cleaner spectra, a radio frequency (RF) matching network, usually employed for producing a more uniform, frequency-independent RF amplitude to suppress artifacts and distortions of the spectral baseline, was omitted. Our optimization of the experimental conditions rationalizes spectral differences from earlier published Q-band data[5, 12, 13], in which the higher frequency resonances (> ≈140 MHz) were comparatively suppressed, their maxima appearing shifted to somewhat lower frequencies (Fig. S3).[*] This is reflected in the fitted hyperfine tensor components reproducing these spectra. While the magnitudes $A_{i,\mathrm{iso}}$ of the four ^{55}Mn hyperfine tensors are approximately the same as those determined in PSII from higher plants and cyanobacteria,[5, 9, 10, 12, 13] the size of the effective anisotropic components $A_{i,\mathrm{aniso}}$ differ. This can be rationalized spectrally by the intensity profiles of the actual ^{55}Mn-ENDOR signals, specifically the relative enhancement of the two peaks at highest radio frequencies, yielding a more isotropic largest hyperfine tensor A_1. This in turn requires the other three tensors A_2, A_3 and A_4 to be less isotropic. Furthermore, reduced orientation selectivity, by employing harder, *i.e.* shorter microwave pulses (π: 32 ns *vs.* 80 ns in Ref.[12]) with a broader excitation width, and a more central field position (1220 mT *vs.* 1260 mT)[12] led to more similar spectra of the native and Sr^{2+}-substituted S_2 state (Fig. 3D in the main text), as also observed for the native and NH_3-modified S_2 state[5]. This pronounced similarity confirms the structural homogeneity among all three cluster types.

Similar to the high RF region, the RF power may be not entirely uniform also at smaller frequencies such that the ENDOR intensities are not quantitative. This may be the reason why the edge of the ^{55}Mn-ENDOR feature ranging from ≈85 to ≈95 MHz cannot be correctly reproduced by the simulations (main text Fig. 3).

---

[*] It is noted that this behaviour stands in contrast to the effect of RF matching on ^{55}Mn-ENDOR resonances observed at a commercial Bruker W-band ENDOR setup in the laboratory of the Bittl group. It is reported that, in the RF range >180 MHz, the peaks intensities are suppressed with increasing radio frequencies and the maxima shifted to lower radio frequencies in the absence of a RF matching network.14. S. Pudollek, Doctoral Thesis, Freie Universität Berlin, 2012.

S7 Electronic structures: exchange couplings and spin states of the BS-DFT models

Table S1 Calculated magnetic parameters for the broken-symmetry (BS) density functional theory (DFT) models of the for S_2 state variants described in the main text (sections 3.1 and 3.3), including total spins S of the ground state (GS) and the first excited state (ES) and the energy difference ΔE between these spin states. Listed are also the differences of the electronic exchange coupling constants J_{ij} and energy gaps between the Sr^{2+}- and Ca^{2+}-containing models Δ(Sr−Ca) and the NH_3- and W1-containing models $\Delta(NH_3-W1)$. J_{ij} and ΔE are given in wavenumbers (cm^{-1}).

	Ca	Sr	$CaNH_3$	$SrNH_3$	Δ(Sr−Ca)		Δ(NH_3−W1)	
					W1	NH_3	Ca	Sr
J_{CD} (J_{12})	−15.7	−17.6	−15.5	−17.4	−1.9	−2.0	−15.7	−17.6
J_{BD} (J_{13})	2.0	1.5	5.0	4.7	−0.5	−0.3	2.0	1.5
J_{AD} (J_{14})	0.8	0.9	0.2	0.3	0.1	0.1	0.8	0.9
J_{BC} (J_{23})	23.8	19.3	27.5	22.6	−4.6	−5.0	23.8	19.3
J_{AC} (J_{24})	1.9	1.9	1.3	1.4	0.0	0.2	1.9	1.9
J_{AB} (J_{34})	−15.9	−16.0	−11.9	−11.9	−0.2	0.1	−15.9	−16.0
S_{GS}	1/2	1/2	1/2	1/2			1/2	1/2
S_{ES}	3/2	3/2	3/2	3/2			3/2	3/2
ΔE_{DFT}	23.5	26.3	16.8	19.0	+2.8	+2.2	23.5	26.3
ΔE_{exp}	23.5[12]	26.5[12]	30-34[15, 16] [a]		+3.0		—[a]	

[a] For the $CaNH_3$ form of the S_2 state, ΔE was determined on PSII preparations isolated from higher plants (spinach), in contrast to the samples of the Ca and Sr forms, which were isolated from cyanobacterial PSII (*T. elongatus*). Thus, their values are not suited for direct comparison and no difference was calculated.

S8 The Mn_{D1}–His332-imino-N interaction: Q-band three-pulse ESEEM, Q-band HYSCORE, W-band EDNMR and simulations

S8.1 τ- and field-dependent Q-Band three-pulse ESEEM spectra

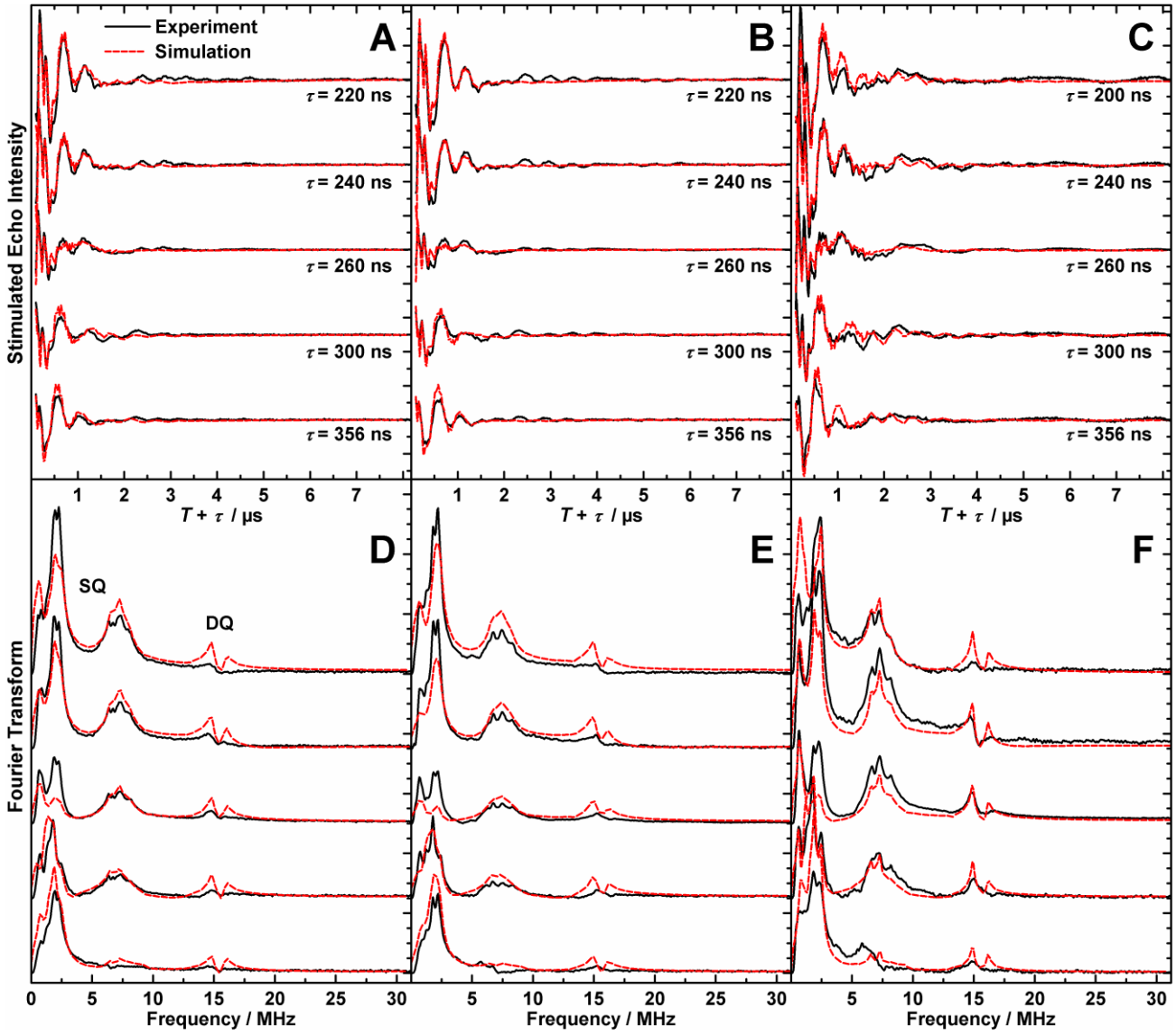

Fig. S4 Q-band three-pulse ESEEM light-minus-dark spectra of the S_2 state Mn_4O_5Ca (A, D), S_2 state Mn_4O_5Sr (B, E) and annealed S_2 state Mn_4O_5Ca–NH_3 (C, F) clusters in PSII isolated from *T. elongatus* at various τ values. **(A–C)** Time-domain spectra and **(D–F)** corresponding Fourier transforms. Black solid traces depict the baseline-corrected experimental spectra; superimposing red dashed traces represent simulations based on the spin Hamiltonian formalism as outlined in sections 2.3 in the main text, S3, S4 and S8.4. The optimized parameter sets are listed in Table 3 of the main text and in detail in

Table S2. ‘SQ’ and ‘DQ’ refer to the position of single and double-quantum transitions, respectively. For a description of the background subtraction procedure, see section S2. The data from the Mn_4O_5Ca and Mn_4O_5Ca–NH_3 samples at τ = 240-300 ns were originally reported in Ref.[5] and reprocessed for this work. Experimental parameters: microwave frequencies: 34.0368 GHz (Ca^{2+}), 34.0433 GHz (Sr^{2+}), 34.0151 GHz (NH_3); magnetic fields: 1220, 1222 mT; shot repetition time: 1 ms; microwave pulse length ($\pi/2$): 12 ns; τ: 220–356 ns (Ca^{2+}, Sr^{2+}), 200–356 ns (NH_3); ΔT: 100 ns; temperature: 5.2 K.

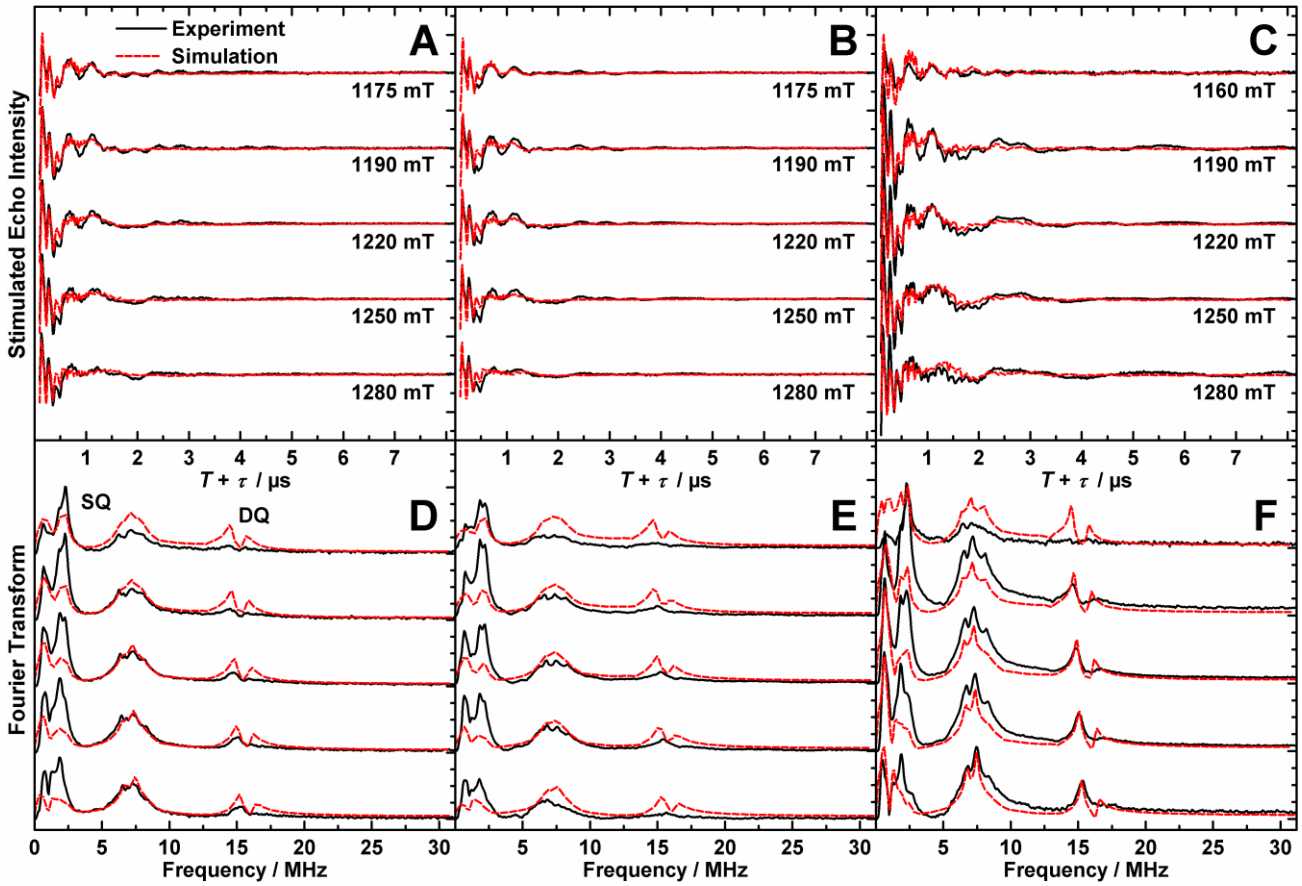

Fig. S5 Q-band three-pulse ESEEM light-minus-dark spectra of the S_2 state Mn_4O_5Ca (A, D), S_2 state Mn_4O_5Sr (B, E) and annealed S_2 state Mn_4O_5Ca–NH_3 (C, F) clusters in PSII isolated from *T. elongatus* at selected magnetic-field positions across the multiline spectrum. **(A–C)** Time-domain spectra and **(D–F)** corresponding Fourier transforms. Black solid traces depict the baseline-corrected experimental spectra; superimposing red dashed traces represent simulations based on the spin Hamiltonian formalism as outlined in sections 2.3 in the main text, S3, S4 and S8.4. The optimized parameter sets are listed in Table 3 of the main text and in detail in Table S2. The labels 'SQ' and 'DQ' refer to the position of single and double-quantum transitions, respectively. For a description of the background subtraction procedure, see section S2. Experimental parameters: microwave frequencies: 34.0368 GHz (Ca^{2+}), 34.0433 GHz (Sr^{2+}), 34.0151 GHz (NH_3); magnetic fields: 1175–1280 mT (Ca^{2+}, Sr^{2+}), 1160–1280 mT (NH_3); shot repetition time: 1 ms; microwave pulse length ($\pi/2$): 12 ns; τ: 260 ns; ΔT: 100 ns; temperature: 5.2 K.

S8.2 Q-band HYSCORE spectra at low and high magnetic-field positions

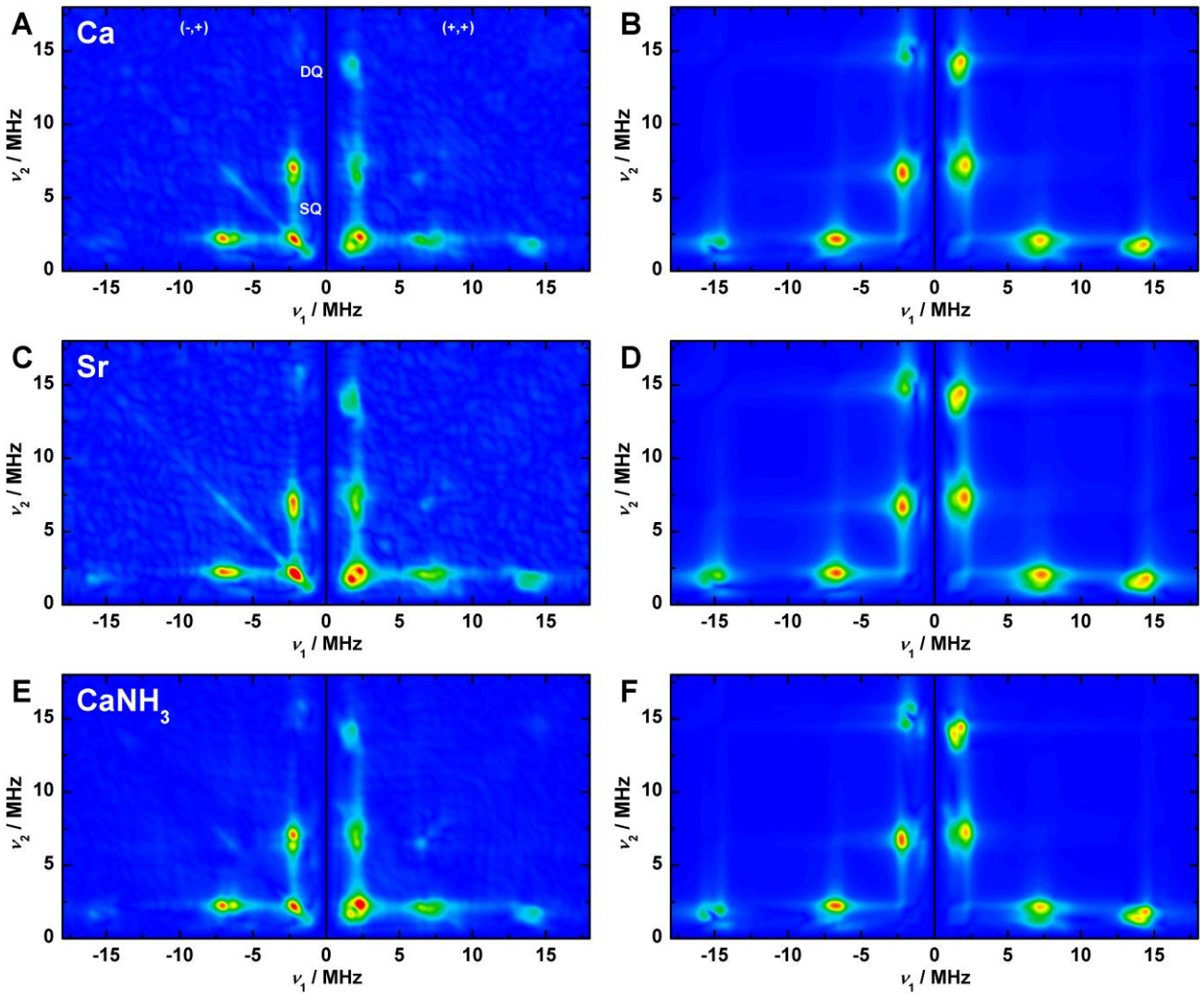

Fig. S6 (-,+) and (+,+) quadrants of the Fourier-transformed Q-band HYSCORE experimental spectra (A, C, E) and simulations (B, D, F) of the S_2 state Mn_4O_5Ca (A, B), S_2 state Mn_4O_5Sr (C, D) and annealed S_2 state Mn_4O_5Ca-NH_3 (E, F) clusters in PSII isolated from *T. elongatus*, measured at the low field edge of the corresponding Q-band multiline spectra. The labels 'SQ' and 'DQ' indicate the regions of single and double quantum transitions, respectively. The optimized parameter sets for the simulations, as described in sections 2.3 in the main text, S3, S4 and S8.4, are listed in Table 3 of the main text and in detail in Table S2. Experimental parameters: microwave frequencies: 34.0222 GHz (Ca^{2+}), 34.0425 GHz (Sr^{2+}), 34.0153 GHz (NH_3); magnetic field: 1175 mT; other settings were those given in Fig. 5 in the main article.

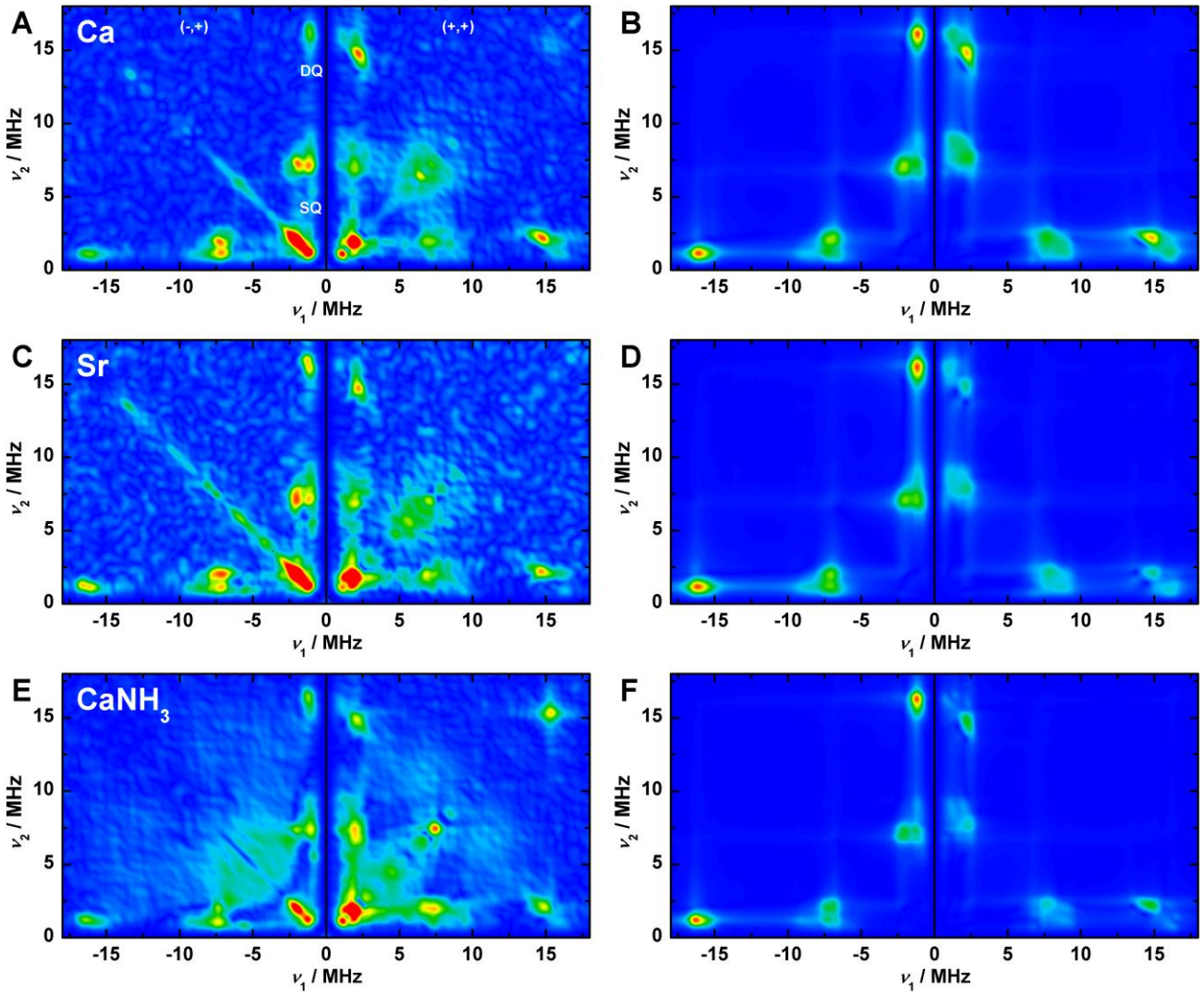

Fig. S7 (-,+) and (+,+) quadrants of the Fourier-transformed Q-band HYSCORE experimental spectra (A, C, E) and simulations (B, D, F) of the S_2 state Mn_4O_5Ca (A, B), S_2 state Mn_4O_5Sr (C, D) and annealed S_2 state Mn_4O_5Ca-NH_3 (E, F) clusters in PSII isolated from *T. elongatus*, measured at the high field edge of the corresponding Q-band multiline spectra. The labels 'SQ' and 'DQ' indicate the regions of single and double quantum transitions, respectively. The optimized parameter sets for the simulations, as described in sections 2.3 in the main text, S3, S4 and S8.4, are listed in Table 3 of the main text and in detail in Table S2. Experimental parameters: microwave frequencies: 34.0227 GHz (Ca^{2+}), 34.0428 GHz (Sr^{2+}), 34.0153 GHz (NH_3); magnetic field: 1260 mT; other settings were those given in Fig. 5 in the main article.

S8.3 W-band ^{14}N- and ^{15}N-ELDOR-detected NMR experiments

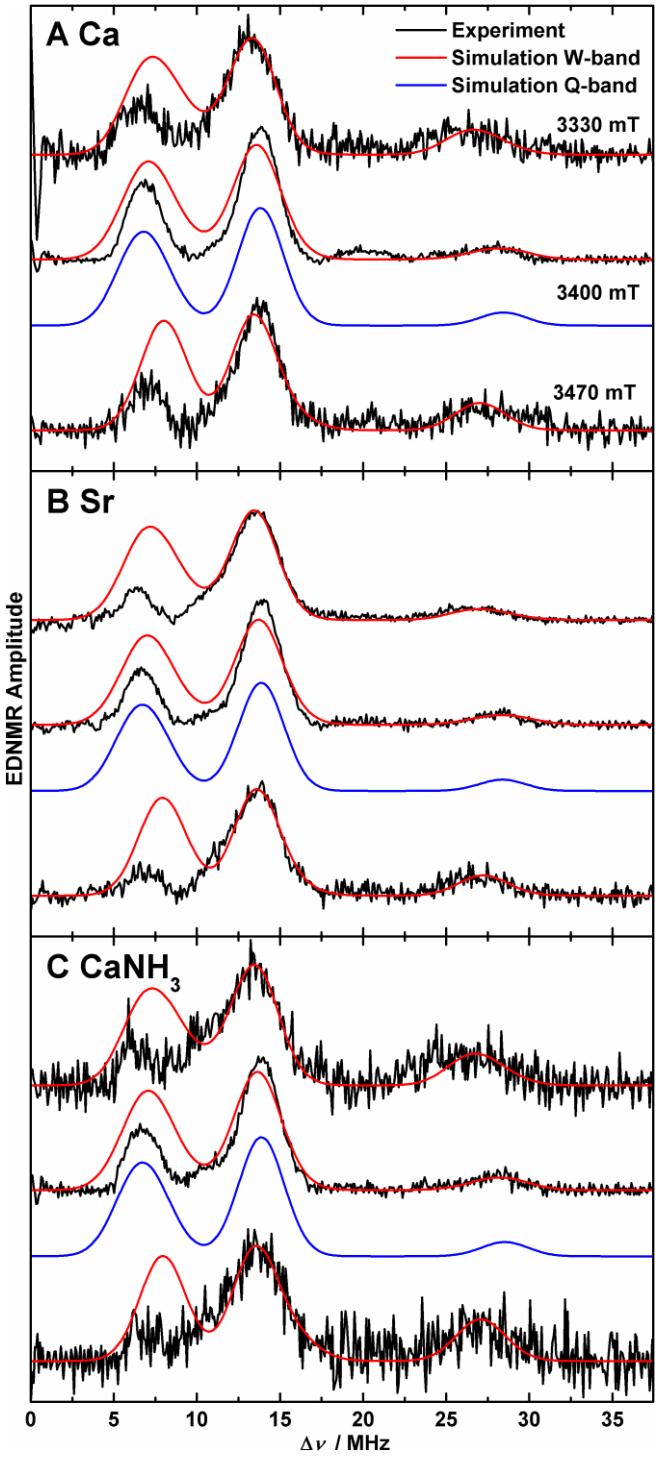

Fig. S8 W-band EDNMR spectra of illuminated **A)** native ^{14}N-PSII (Mn_4O_5Ca S_2), **B)** Sr^{2+}-substituted ^{14}N-PSII (Mn_4O_5Sr S_2) and **C)** NH_3-modified ^{14}N-PSII (Mn_4O_5Ca–NH_3 S_2) samples isolated from *T. elongatus*. Black solid traces depict the baseline-corrected experimental spectra, red and blue solid traces represent simulations based on the spin Hamiltonian formalism (see sections 2.3 in the main text, S3 and S4). The optimized parameter sets are listed in Table S2. The spectra displayed in each panel

were measured or simulated at the low field edge, the center field and the high field edge (top to bottom) of the corresponding W-band multiline EPR spectra (Fig. 3C in the main text). The data from the native S_2 state were originally published in Ref.[1] and were reprocessed to allow comparison to the two chemically modified samples. Experimental parameters: microwave frequencies: 94.011 (A), 93.978 GHz (B), 94.066 GHz (C); magnetic fields: 3.33 T (top), 3.4 T (center), 3.47 T (bottom); shot repetition time: 1.5 ms; microwave pulse length (π): 400 ns; high turning angle pulse length t_{HTA}: 14 μs; τ: 500 ns; temperature: 4.8 K.

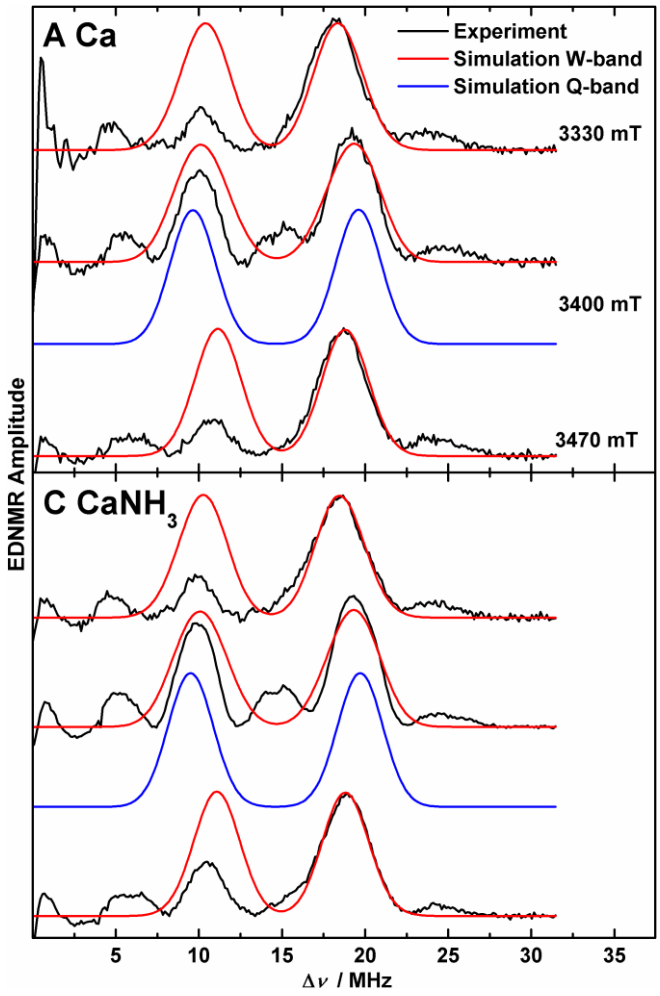

Fig. S9 Field-dependent W-band EDNMR spectra of illuminated **A)** native ^{15}N-PSII (Mn_4O_5Ca S_2), **B)** NH_3-modified ^{15}N-PSII (Mn_4O_5Ca–NH_3 S_2) samples isolated from *T. elongatus*. Black solid traces depict the baseline-corrected experimental spectra, red and blue solid traces represent simulations based on the spin Hamiltonian formalism (see sections 2.3 in the main text, S3 and S4). The optimized parameter sets are listed in Table S2. The spectra displayed in each panel were measured or simulated at the low field edge, the center field and the high field edge (top to bottom) of the corresponding W-band multiline EPR spectra (Fig. 3C in the main text). Experimental parameters: microwave frequencies: 94.022 GHz (A), 93.996 GHz (B); magnetic fields: 3.33 T (top), 3.4 T (center), 3.47 T (bottom); shot repetition time: 0.5 ms; microwave pulse length (π): 160 ns; t_{HTA}: 8 µs; τ: 500 ns; temperature: 4.8 K.

Both the ^{14}N and ^{15}N spectra are highly similar for the native, Sr^{2+}-substituted and NH_3-modified S_2 states. The three systems exhibit identical orientation dependencies, with the clearly largest splitting at the central field position ($g \approx 1.98$) and smaller splittings at the low- and high-field edges ($g \approx 2.02$ and $g \approx 1.94$, respectively). This behaviour is shown by both the ^{14}N and ^{15}N signals of the His332 imino-N. At the outer magnetic-field positions, the hyperfine splittings are approximately of the same size. The general similarity of the ^{14}N orientation selectivity to that of the ^{15}N signals results from the fact that the hyperfine coupling is the dominant electron-nuclear interaction and the magnitude of the NQI is considerably smaller. Despite the similar overall field-dependence, there are differences in the exact positions of the peaks, most prominent for the double-quantum transitions, at a certain magnetic field between the three variants of the S_2 state.

S8.4 Magnetic parameters of the His332 imino-^{14}N interactions with the S_2 state OEC forms

Table S2 Effective/projected ^{14}N hyperfine and NQI tensors in MHz for the interaction of the His332 imino-N with the Mn_4O_5Ca, Mn_4O_5Sr and annealed Mn_4O_5Ca–NH_3 clusters in the S_2 state in PSII from *T. elongatus* and parameters from previous studies on various species. The Q-band ESEEM/HYSCORE (Figs. 5 in the main text, S4, S5, S6 and S7) and the W-band EDNMR (Figs. S8, S9) simulations employed two different *A* tensors for a given spin system, while the NQI tensor and the Euler angle rotations of the hyperfine and NQI tensor were identical for the two frequencies.

S_2 state	Method	$\lvert A_1\rvert$	$\lvert A_2\rvert$	$\lvert A_3\rvert$	$\lvert A_{iso}\rvert$[a]	A_{dip}[b]	A_η[c]	$\lvert e^2Qq/h\rvert$	η[c]
Native	Q-Band[d]	5.6	8.4	7.2	7.1	0.75	0.81	1.97	0.75
	W-band[d]	3.2	9.2	6.7	6.3	1.59	0.80		
	BS-DFT[e]	4.6	5.9	6.8	5.8	0.59	0.74	1.65	0.91
Sr^{2+}-substituted	Q-Band[d]	5.9	8.5	7.4	7.3	0.69	0.83	1.98	0.79
	W-band[d]	3.4	9.6	6.8	6.6	1.58	0.87		
	BS-DFT[e]	4.7	6.1	6.8	5.8	0.57	0.61	1.65	0.91
NH_3-modified	Q-Band[d]	5.7	8.6	7.3	7.2	0.75	0.89	1.96	0.80
	W-band[d]	3.5	9.1	6.6	6.4	1.45	0.86		
	BS-DFT[e]	4.7	6.1	7.5	6.1	0.71	0.99	1.68	0.88
Native, spinach[17]	X-, P-, K_a-band	6.3, 7.8, 7.8			7.3	0.5	0	1.98	0.84
Native, *Synechocystis* sp. PCC 6803[18]	K_a-, Q-band[f]	5.45, 7.15, 8.25			6.95	0.75	0.73	1.98	0.82
Native[1]	W-band[g]	3.8	7.7	6.2	5.9	1.1	0.71	0	0

[a] A_{iso} is defined as the average of the principal components of the hyperfine tensor: $A_{iso} = (A_1 + A_2 + A_3)/3$. [b] A_{dip} is defined in terms of T_1, T_2, and T_3 as $A_{dip} = (T_1 + T_2)/2 = -T_3/2$. [c] The rhombicity is defined by A_η or $\eta = (T_1 - T_2)/T_3$, respectively. T_1, T_2, and T_3 represent the three principal components of the hyperfine tensors minus A_{iso} and of the NQI tensors and are labeled such that $|T_1| \le |T_2| \le |T_3|$. [d] The Euler rotation angles [α, β, γ] are [0, 45, 0]°, [0, 45, 0]° and [0, 44, 0]° for the *A* tensors and [20, −57, 0]°, [18, −54, 0]° and [16, −60, 0]° for the NQI tensors of the Mn_4O_5Ca, Mn_4O_5Sr and Mn_4O_5Ca–NH_3 clusters,

respectively. [e] Their calculated orientations are such that the smallest, medium and large effective components are aligned approximately (angular deviation < 6°) along the Mn_{D1}–His332, the Mn_{D1}-O3 and the Mn_{D1}–Asp342, respectively (Fig. S10, main text Fig. 1). By definition, the large components along the Jahn-Teller axis were assigned to A_3 and, by inspection, the others to A_1 and A_2. [f] The Euler rotation angles [α, β, γ] of the NQI tensor are [−30, 0, 40]°. [g] Euler rotation angles [α, β, γ] of the hyperfine tensor were [0, 30, 0]°.

A simultaneous fitting of all Q-band three-pulse ESEEM (Figs. S4, S5) and HYSCORE (Figs. 5 in the main text, S6 and S7) spectra and W-band ^{14}N- and, if available, ^{15}N-EDNMR spectra (Figs. S8 and S9) of the native, the Sr^{2+}-substituted and the NH_3-modified S_2 state was performed using the spin Hamiltonian formalism (see Materials and Methods section 2.3 and sections S3 and S4). Only one nitrogen nucleus was included representing the coordinating imino-N in the imidazole ring of His332. Non-coordinating nitrogens do not contribute significantly to the ESEEM and HYSCORE modulations and the EDNMR spectra (see also Figs. S8 and S9).[1, 17, 19] As the relative intensities of single- and double-quantum transition lines in EDNMR experiments are highly dependent on an experimental parameter, namely the high turning angle (HTA) pulse, single- and double-quantum transitions were calculated and normalized separately in the simulations, as in Rapatskiy *et al.*[1] and Pérez Navarro *et al.*[5]. The fitted effective ^{14}N *A* and NQI tensors are listed in Table S2. In case of the ^{15}N EDNMR spectra, the *A* tensor components were scaled by the ratio of the nuclear *g* values of ^{14}N and ^{15}N (and no NQI is effective). The effective *G* tensors used were the same as those determined by the EPR and ^{55}Mn-ENDOR simulations (Table 1 in the main text).

In simulations where the entire Q-band ESEEM/HYSCORE dataset was included, a single, consistent parameter set could be obtained. The fitted hyperfine and NQI parameters of all three S_2 state variants are very similar to those reported in higher plant and mesophilic cyanobacterial (*Synechocystis* sp. PCC 6803) PSII by the Britt laboratory[17, 18] (Table S2). These simulations though do not constrain the orientation of the hyperfine tensor orientations relative to the *G* matrix. The inclusion of the high-

frequency W-band EDNMR data allows the relative tensor orientations to be ascertained. However, the hyperfine tensors found to reproduce the field dependence of the W-band EDNMR dataset do not reproduce the Q-band ESEEM and HYSCORE data but instead comprise a smaller isotropic and a larger dipolar component. As the blue solid traces in Figs. S8 and S9 show, the splitting of the peaks in the W-band EDNMR spectra is overestimated when employing the hyperfine tensors fitted to the Q-band ESEEM and HYSCORE data, already to a smaller extent at the center field and more drastically at the edge position. Since our simulations of the W-band EDNMR signals now explicitly include the NQI term, the omission of this term cannot be the reason for this apparent mismatch. A rationale for this difference is given in the main text section 3.4. Despite the differences of the size of the dipolar component A_{dip} of the nitrogen hyperfine interaction between the Q- and W-band simulations, for all three S_2 state variants, their rhombicities A_η are very similar.

For the three forms of the S_2 state, the hyperfine tensors were required to be rotated about −45° around the y axis, relative to the orientation of the effective *G* tensors, which resulted to be rhombic from the simulations of the EPR/^{55}Mn ENDOR spectra in this work (main text section 3.2). This is similar to the simulation of the ^{14}N-EDNMR spectra at W-band of the native S_2 state in Ref.[1]. This rotation results from the fact that approximately the same peak splittings are present in the W-band EDNMR spectra recorded at the edge positions of the S_2 multiline, corresponding to the x and z axes in the *G* tensor frame. Thus, the hyperfine coupling is expected to be small along G_x and G_z and large along G_y. However, the effective ^{14}N/^{15}N hyperfine tensor cannot be axial, as inferred from the ESEEM and HYSCORE spectra. Hence, it is supposed that the *A* tensor of the imino-^{14}N/^{15}N and the molecular *G* tensor are not collinear. A β angle rotation in the xz plane (Fig. S10) allows the EDNMR data to be fit employing a rhombic hyperfine tensor, as noted earlier in Ref.[1]. The simulations also afforded rotations of the NQI tensor around the z axis (α = 16 to 20°) and the y' axis (β = −54 to −60°). Upon a switch of the values of A_1 and A_3 and use of β = 45° − 90° = −45°, generating the same simulation traces, it becomes obvious that the orientations of NQI and hyperfine tensors are relatively similar, as observed in previous simulations of K_a- and Q-band three-pulse ^{14}N and ^{15}N-ESEEM data of this His332 imino-N.[18]

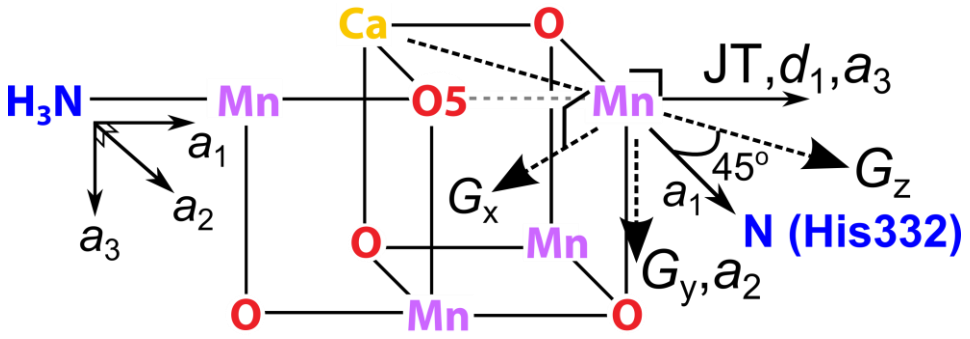

Fig. S10 Proposed orientations of the His332 imino-$^{14}N/^{15}N$ and $^{14}NH_3$ hyperfine tensors relative to the fine structure tensor of the Mn_{D1}^{III} ion *d* and the molecular *G* frame in a schematic model of the Mn_4O_5Ca–NH_3 cluster. a_1, d_1 and G_z define the unique tensor axis, 'JT' denotes the Jahn-Teller axis of Mn_{D1}^{III}.

S9 X-band ^{14}N- and ^{15}N-three pulse ESEEM experiments on the NH_3-modified S_2 state

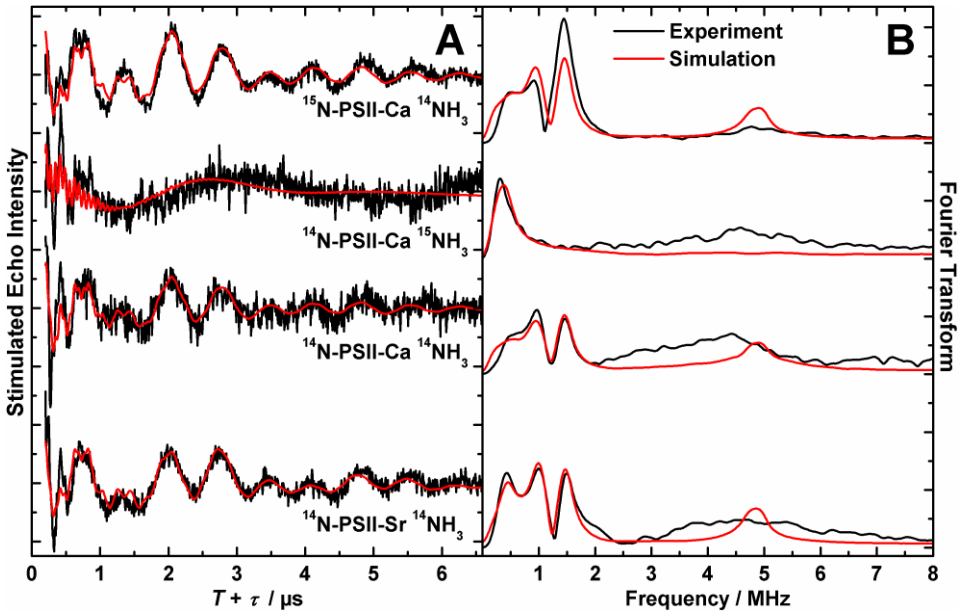

Fig. S11 X-band three-pulse ESEEM light-minus-dark spectra of $^{14}NH_3$-modified native ^{15}N-PSII, $^{15}NH_3$-modified native ^{14}N-PSII, $^{14}NH_3$-modified native ^{14}N-PSII and $^{14}NH_3$-modified Sr^{2+}-substituted ^{14}N-PSII (top to bottom) samples isolated from *T. elongatus* in the annealed S_2 state. **A)** Time-domain spectra and **B)** corresponding Fourier transforms. Black traces depict the baseline-corrected experimental spectra (see section S2); superimposing red traces represent simulations based on the spin Hamiltonian formalism (see sections 2.3 in the main text, S3 and S4). The optimized parameter sets are listed in Table S3. The ^{15}N-PSII-Ca $^{14}NH_3$ and ^{14}N-PSII-Ca $^{14}NH_3$ data were originally presented in Pérez Navarro *et al.*[5] and reprocessed for this work. Experimental parameters: microwave frequencies: 9.680 GHz, 9.674 GHz, 9.684 GHz, 9.681 GHz (top to bottom); magnetic field: 333 mT; shot repetition time: 8.16 ms; microwave pulse length ($\pi/2$): 8 ns; τ: 136 ns (A), average of experiments with 136, 152, 168, 184 ns (B); ΔT: 64 ns; temperature: 4.3 K.

Table S3 Fitted (X-band three-pulse ESEEM, Fig. S11) and calculated effective/projected ^{14}N hyperfine and NQI tensors, listed as absolute values in MHz, for the electron-nuclear coupling of the NH_3 bound in the annealed Mn_4O_5Ca–NH_3 and Mn_4O_5Sr–NH_3 S_2 state clusters in PSII from *T. elongatus* and, from earlier studies, higher plant spinach.

S_2 state	Method	$\lvert A_1\rvert$	$\lvert A_2\rvert$	$\lvert A_3\rvert$	$\lvert A_{iso}\rvert^a$	$A_{dip}{}^b$	$A_\eta{}^c$	$\lvert e^2Qq/h\rvert$	η^c
Mn_4O_5Ca–NH_3	ESEEM	1.69	2.76	2.62	2.36	0.33	0.22	1.52	0.47
	BS-DFT	3.97	2.01	2.04	2.68	-0.65	0.02	0.94	0.87
Mn_4O_5Sr–NH_3	ESEEM	1.81	2.72	2.59	2.37	0.28	0.23	1.58	0.45
	BS-DFT	3.87	2.07	2.10	2.68	-0.59	0.03	0.93	0.87
Mn_4O_5Ca–NH_3, spinach[20]	ESEEM	1.89	2.49	2.49	2.29	0.20	0.0	1.61	0.59

[a] A_{iso} is defined as the average of the principal components of the hyperfine tensor: $A_{iso} = (A_1 + A_2 + A_3)/3$. [b] A_{dip} is defined in terms of T_1, T_2, and T_3 as $A_{dip} = (T_1 + T_2)/2 = -T_3/2$. [c] The rhombicity is defined by A_η or $\eta = (T_1 - T_2)/T_3$, respectively. T_1, T_2, and T_3 represent the three principal components of the hyperfine tensors minus A_{iso} and of the NQI tensors and are labeled such that $|T_1| \leq |T_2| \leq |T_3|$.

Three-pulse ESEEM experiments were performed at X-band on $^{14}NH_3/^{15}NH_3$-modified (annealed), Ca^{2+}-and Sr^{2+}-containing, wild-type and all-^{15}N-labeled PSII samples in the NH_3-treated S_2 state. Fig. S11 depicts light-minus-dark-corrected time-domain (Fig. S11A) and, to minimize spectral artifacts, τ-averaged frequency-domain (Fig. S11B) spectra at 4.8 K of $^{14}NH_3$-modified native ^{15}N-PSII, $^{15}NH_3$-modified native ^{14}N-PSII, $^{14}NH_3$-modified native ^{14}N-PSII and $^{14}NH_3$-modified Sr^{2+}-substituted ^{14}N-PSII (top to bottom). At X-band frequencies, the echo modulations are dominated by the nitrogen hyperfine interaction of the bound NH_3 as it meets the cancellation condition ($A = 2\nu_n$). Importantly, the His332 imino-N interaction is suppressed as at X-band. Resonances from ^{14}N nuclei ($I = 1$), which exhibit significant NQI contributions in contrast to the ^{15}N nucleus ($I = ½$), appear more prominent in the three-pulse ESEEM data than those from ^{15}N ligands. Thus, the $^{14}NH_3$-modified native ^{15}N-PSII data are dominated by the $^{14}NH_3$ interactions as compared to the ^{15}N His332 resonances, while all ^{14}N-PSII spectra show a broad His332 imino-^{14}N resonance centered at ≈4.6 MHz in the Fourier-transformed spectrum.[5]

Spectral simulations of the X-band time-domain data were performed as described in the Materials and Methods section 2.3 and sections S3 and S4. They also included the ligating imino-^{14}N or -^{15}N nucleus of His332, represented by the fitted Q-band parameters, and contributions from ^{1}H nuclei. The ^{1}H resonances, not displayed in the Fourier transforms, are centered at ≈14.2 MHz and were largely suppressed at a τ length of 136 ns.

The presented BS-DFT calculations confirm the small hyperfine rhombicity, however, yielding a negative dipolar hyperfine component with the unique component being the largest. The non-axiality of the electric field gradient, inferred from the large asymmetry parameter η = 0.47 of the NQI and reproduced by the BS-DFT computations, is attributed to a non-axial H-bonding geometry (main text section 4.1.2b, Fig. 7). In the original work by Britt *et al.*[20], the large η was proposed not to arise from a terminal NH_3 but rather from a less symmetric amido (NH_2) bridge between two Mn and/or the Ca^{2+} ion.

S10 Exchangeable ^{17}O species

S10.1 W-band ^{17}O-ELDOR-detected NMR experiments

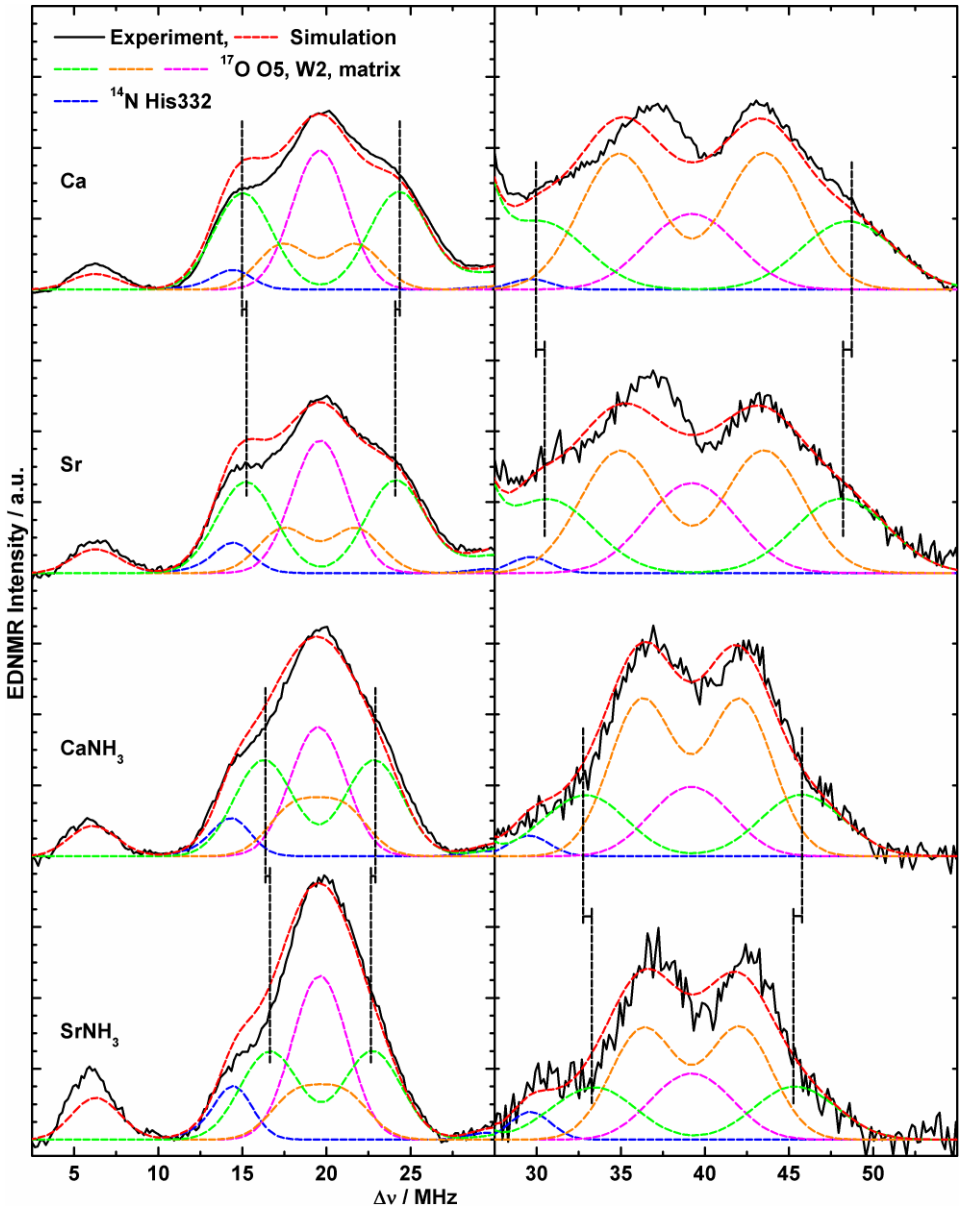

Fig. S12 Single-quantum (left) and double-quantum (right) regions of the ^{17}O-EDNMR spectra of the native (Ca) the Sr^{2+}-substituted (Sr), the NH_3-annealed ($CaNH_3$) and the Sr^{2+}-substituted NH_3-annealed ($SrNH_3$) S_2 states in PSII samples isolated from *T. elongatus*. The double-quantum envelopes are presented on a 4 times expanded vertical scale as compared to the single quantum resonances. Black solid traces show the background-corrected experimental spectra; superimposing red dashed traces represent simulations based on the spin Hamiltonian formalism as outlined in sections 2.3 in the main text, S3, S4. Coloured dashed lines represent a decomposition of the simulation showing contributions

from the individual ^{14}N and ^{17}O nuclei. Black dashed lines, visualizing the shift of the fitted single- and double-quantum transition peaks, highlight the decrease of the strong ^{17}O interaction, assigned to the μ-oxo bridge O5, upon substitution of the Ca^{2+} for a Sr^{2+} ion. The optimized parameter sets are listed in Table S4. Same as for the ^{14}N- and ^{15}N-EDNMR signals, the single- and double-quantum resonances of each ^{17}O species were weighted and normalized individually. In the simulations, the double-quantum peaks ν_α and ν_β of the individual ^{17}O species were required to be equal, unlike in Refs.[1, 5], where an intensity imbalance was allowed for. The data from the NH_3-treated S_2 state were originally published in Ref.[1] and were reprocessed to allow comparison to the other S_2 state forms. Experimental parameters: microwave frequencies: 93.988 (Ca), 94.033 GHz (Sr), 94.069 GHz (CaNH3), 93.964 GHz (SrNH3); magnetic field: 3.4 T; shot repetition time: 1.5 ms; microwave pulse length (π): 400 ns; t_{HTA}: 14 μs; τ: 500 ns; temperature: 4.8 K..

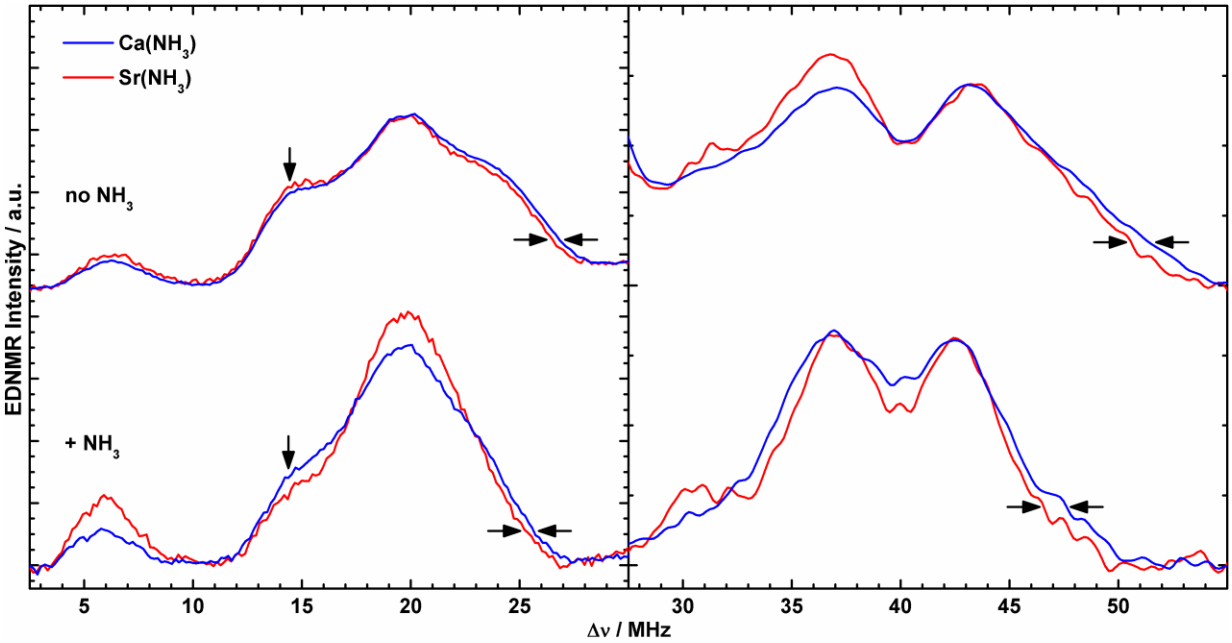

Fig. S13 Effect of Ca^{2+}/Sr^{2+} exchange on the single-quantum (left) and double-quantum (right) envelopes of the ^{17}O-EDNMR spectra of the not NH_3-treated (top) and NH_3-annealed (bottom) S_2 states in PSII samples isolated from *T. elongatus*. The blue traces depict the Ca^{2+}-containing Mn_4O_5Ca and Mn_4O_5Ca-NH_3 clusters, red traces represent the Sr^{2+}-containing Mn_4O_5Sr and Mn_4O_5Sr-NH_3 clusters. The double-quantum envelopes are presented on a 4.5 times expanded vertical scale as compared to the single quantum resonances. They were smoothed using a 9-point moving average and normalized with respect to the high-frequency doublet peak around 43 MHz for better comparability. As pointed out by the horizontal arrows, Sr^{2+} substitution results in a systematic narrowing of the single- and double quantum envelopes in both the S_2 states without and with NH_3 bound to the Mn cluster. The vertical arrows mark the maximum of the underlying ν_β peaks of the His332 imino-^{14}N, which prevent the low-frequency edges of the ^{17}O single-quantum envelopes and thus their differences from being resolved. Experimental parameters: see Fig. S12.

Table S4 Fitted effective ^{17}O hyperfine tensors, listed as absolute values in MHz, from W-band EDNMR experiments (Fig. 6 in the main text and Fig. S12) for the electron-nuclear coupling of the oxygen species exchangeable in the S_1 state with the Mn_4O_5Ca, Mn_4O_5Sr, $Mn_4O_5Ca–NH_3$ and $Mn_4O_5Sr–NH_3$ S_2 state clusters in PSII from *T. elongatus*. A_1, A_2 and A_3 are the principal components of the hyperfine tensor, which are not assigned to the principal axes of the coordinate system defined by the *G* tensor.

S_2 state	Oxygen	$\|A_1\|$, $\|A_2\|$, $\|A_3\|$	$\|A_{iso}\|$[a]	A_{dip}[b]	A_η[c]
all	matrix	2.1, 0.2, 2	1.4	0.6	0.08
Mn_4O_5Ca	W2	5.1, 5.1, 3.3	4.5	0.6	0.08
	O5	10.7, 5.3, 13.1	9.7	2.2	0.55
Mn_4O_5Sr	W2	5.1, 5.1, 3.3	4.5	0.6	0.08
	O5	10.2, 4.8, 12.6	9.2	2.2	0.55
$Mn_4O_5Ca–NH_3$	W2	3.7, 3.7, 1.9	3.1	0.6	0.08
	O5	8.0, 2.6, 10.4	7.0	2.2	0.55
$Mn_4O_5Sr–NH_3$	W2	3.7, 3.7, 1.9	3.1	0.6	0.08
	O5	7.5, 2.1, 9.9	6.5	2.2	0.55

[a] A_{iso} is defined as the average of the principal components of the hyperfine tensor: $A_{iso} = (A_1 + A_2 + A_3)/3$. [b] A_{dip} is defined in terms of T_1, T_2, and T_3 as $A_{dip} = (T_1 + T_2)/2 = -T_3/2$. [c] The rhombicity is defined by A_η or $\eta = (T_1 - T_2)/T_3$, respectively. T_1, T_2, and T_3 represent the three principal components of the hyperfine tensors minus A_{iso} and of the NQI tensors and are labeled such that $|T_1| \leq |T_2| \leq |T_3|$.

S10.2 X-band CW EPR experiments in the absence and presence of $H_2{}^{17}O$

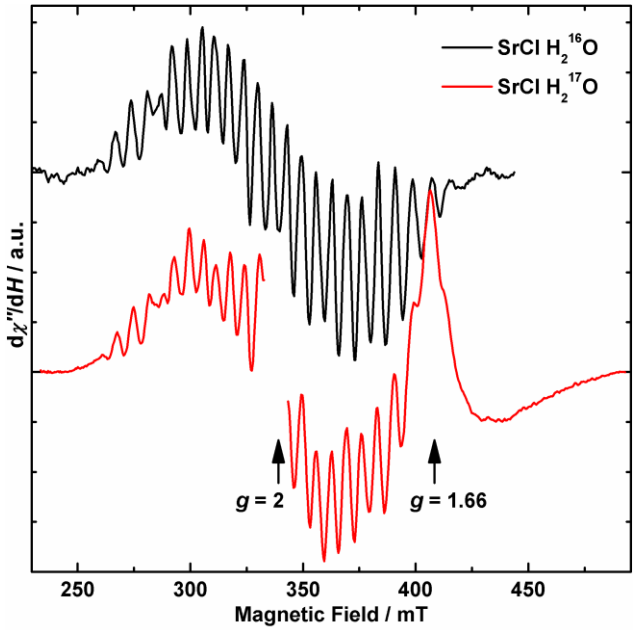

Fig. S14 X-band CW EPR spectra of the Sr^{2+}-substituted S_2 state in PSII samples in the absence (black) and presence (red) of $H_2{}^{17}O$ showing no line broadening upon ^{17}O exchange. The spectrum in the not $H_2{}^{17}O$ -enriched buffer was taken from Cox *et al.*[12]. In the spectrum of the $H_2{}^{17}O$-exchanged PSII sample, the $Y_D^{\bullet}$ signal centered at about $g \approx 2$ was removed for clarity of presentation; the underlying comparatively narrow signal centered at $g \approx 1.66$ originates from the semiquinone-iron in the $Q_A^{-}Fe^{2+}Q_B^{-}$ state.[21, 22] Experimental parameters: microwave frequencies: 9.4213 GHz (no ^{17}O); 9.4989 GHz (with ^{17}O); microwave power: 20 mW; modulation amplitude: 25 G; time constant: 82 ms; temperature: 8.6 K.

S11 References

1. L. Rapatskiy, N. Cox, A. Savitsky, W. M. Ames, J. Sander, M. M. Nowaczyk, M. Rögner, A. Boussac, F. Neese, J. Messinger and W. Lubitz, *J. Am. Chem. Soc.*, 2012, **134**, 16619-16634.
2. S. Stoll and A. Schweiger, *J. Magn. Reson.*, 2006, **178**, 42-55.
3. S. Stoll and R. D. Britt, *Phys. Chem. Chem. Phys.*, 2009, **11**, 6614-6625.
4. N. Cox, W. Lubitz and A. Savitsky, *Mol. Phys.*, 2013, **111**, 2788-2808.
5. M. Pérez Navarro, W. M. Ames, H. Nilsson, T. Lohmiller, D. A. Pantazis, L. Rapatskiy, M. M. Nowaczyk, F. Neese, A. Boussac, J. Messinger, W. Lubitz and N. Cox, *Proc. Natl. Acad. Sci. U. S. A.*, 2013, **110**, 15561-15566.
6. V. K. Yachandra, K. Sauer and M. P. Klein, *Chem. Rev.*, 1996, **96**, 2927-2950.
7. J. Messinger, J. H. Robblee, U. Bergmann, C. Fernandez, P. Glatzel, H. Visser, R. M. Cinco, K. L. McFarlane, E. Bellacchio, S. A. Pizarro, S. P. Cramer, K. Sauer, M. P. Klein and V. K. Yachandra, *J. Am. Chem. Soc.*, 2001, **123**, 7804-7820.
8. M. Haumann, C. Müller, P. Liebisch, L. Iuzzolino, J. Dittmer, M. Grabolle, T. Neisius, W. Meyer-Klaucke and H. Dau, *Biochemistry*, 2005, **44**, 1894-1908.
9. J. M. Peloquin, K. A. Campbell, D. W. Randall, M. A. Evanchik, V. L. Pecoraro, W. H. Armstrong and R. D. Britt, *J. Am. Chem. Soc.*, 2000, **122**, 10926-10942.
10. L. V. Kulik, B. Epel, W. Lubitz and J. Messinger, *J. Am. Chem. Soc.*, 2007, **129**, 13421-13435.
11. C. Teutloff, S. Pudollek, S. Kessen, M. Broser, A. Zouni and R. Bittl, *Phys. Chem. Chem. Phys.*, 2009, **11**, 6715-6726.
12. N. Cox, L. Rapatskiy, J.-H. Su, D. A. Pantazis, M. Sugiura, L. Kulik, P. Dorlet, A. W. Rutherford, F. Neese, A. Boussac, W. Lubitz and J. Messinger, *J. Am. Chem. Soc.*, 2011, **133**, 3635-3648.
13. J. H. Su, N. Cox, W. Ames, D. A. Pantazis, L. Rapatskiy, T. Lohmiller, L. V. Kulik, P. Dorlet, A. W. Rutherford, F. Neese, A. Boussac, W. Lubitz and J. Messinger, *Biochim. Biophys. Acta, Bioenerg.*, 2011, **1807**, 829-840.

14. S. Pudollek, Doctoral Thesis, Freie Universität Berlin, 2012.

15. D. Koulougliotis, R. H. Schweitzer and G. W. Brudvig, *Biochemistry*, 1997, **36**, 9735-9746.

16. G. A. Lorigan and R. D. Britt, *Photosynth. Res.*, 2000, **66**, 189-198.

17. G. J. Yeagle, M. L. Gilchrist, R. M. McCarrick and R. D. Britt, *Inorg. Chem.*, 2008, **47**, 1803-1814.

18. T. A. Stich, G. J. Yeagle, R. J. Service, R. J. Debus and R. D. Britt, *Biochemistry*, 2011, **50**, 7390-7404.

19. S. Milikisiyants, R. Chatterjee, A. Weyers, A. Meenaghan, C. Coates and K. V. Lakshmi, *J. Phys. Chem. B*, 2010, **114**, 10905-10911.

20. R. D. Britt, J. L. Zimmermann, K. Sauer and M. P. Klein, *J. Am. Chem. Soc.*, 1989, **111**, 3522-3532.

21. A. R. Corrie, J. H. A. Nugent and M. C. W. Evans, *Biochimica Et Biophysica Acta*, 1991, **1057**, 384-390.

22. C. Fufezan, C. X. Zhang, A. Krieger-Liszkay and A. W. Rutherford, *Biochemistry*, 2005, **44**, 12780-12789.